Semiannual Technical Report

Nitride Semiconductors for Ultraviolet Detection

Supported under Grant #N00014-92-J-1720
Office of the Chief of Naval Research
Report for the period 1/1/95–6/30/95

R. F. Davis, M. D. Bremser, K. Gruss,
K. Linthicum, B. Perry, and T. W. Weeks, Jr.
Materials Science and Engineering Department
North Carolina State University
Campus Box 7907
Raleigh, NC 27695-7907

June, 1995

REPORT DOCUMENTATION PAGE

Form Approved
OMB No. 0704-0188

1. AGENCY USE ONLY *(Leave blank)*	2. REPORT DATE	3. REPORT TYPE AND DATES COVERED
	June, 1995	Semiannual Technical 1/1/95–6/30/95

4. TITLE AND SUBTITLE

Nitride Semiconductors for Ultraviolet Detection

5. FUNDING NUMBERS

s400018srr01
1114SS
N00179
N66005
4B855

6. AUTHOR(S)

Robert F. Davis

7. PERFORMING ORGANIZATION NAME(S) AND ADDRESS(ES)

North Carolina State University
Hillsborough Street
Raleigh, NC 27695

8. PERFORMING ORGANIZATION REPORT NUMBER

N00014-92-J-1720

9. SPONSORING/MONITORING AGENCY NAMES(S) AND ADDRESS(ES)

Sponsoring: ONR, Code 312, 800 N. Quincy, Arlington, VA 22217-5660
Monitoring: Administrative Contracting Officer, Regional Office Atlanta
101 Marietta Tower, Suite 2805
101 Marietta Street
Atlanta, GA 30332-0490

10. SPONSORING/MONITORING AGENCY REPORT NUMBER

11. SUPPLEMENTARY NOTES

12a. DISTRIBUTION/AVAILABILITY STATEMENT

Approved for Public Release; Distribution Unlimited

12b. DISTRIBUTION CODE

13. ABSTRACT ***(Maximum 200 words)***

Monocrystalline, undoped GaN(0001) thin films, free of low-angle grain boundaries and associated oriented domain microstructure, have been grown at 950°C on high-temperature, ≈100 nm thick, monocrystalline AlN(0001) buffer layers pre-deposited at 1100°C on α(6H)-SiC(0001)$_{Si}$ substrates via OMVPE in a cold-wall, vertical, pancake-style reactor. The PL spectra of the GaN films deposited on both vicinal and on-axis substrates revealed a strong donor-bound exciton peak at 357.36 nm with a FWHM value of 4 meV. This peak shifted to lower energies as film thickness increased. The defect peaks were very weak. Undoped films were too resistive for accurate Hall-effect measurements. Controlled n-type, Si-doping in GaN was achieved for net carrier concentrations ranging from approximately 1×10^{17} cm^{-3} to 1×10^{20} cm^{-3}. Annealed (600°C) Mg-doped, p-type GaN was achieved with $n_A - n_D \approx 3 \times 10^{17}$ cm^{-3}, $R \approx 7\ \Omega$·cm and $\mu \approx 3$ cm^2/V·s, as measured by Hall-effect. $Al_xGa_{1-x}N$ films and abrupt heterojunctions have been grown for $0 \le x \le 1$. CL spectra for $x < 0.5$ showed intense near band-edge emission. The shift in the deep-level emission relative to the shift in the band-edge emission as a function of x was measured and compared to past results for pressure studies of GaN. As-deposited Si-doped $Al_{0.75}Ga_{0.25}N$ exhibited a negative electron affinity. A new method for the growth of III-V compounds, namely, the use of a high temperature catalytic ammonia cracker cell, has been designed and tested for use with GSMBE to minimize the film damage that occurs from ECR. Preliminary testing of the cracker and initial AlN and GaN growth results are presented. The GaN films have been reactively ion etched in Cl_2 and BCl_3 plasmas using varying flow rates, pressures, power and DC bias. Typical etching parameters were: 1-10 sccm total gas flow, 35-75 mtorr, 125-200 W power and -(200-300)V bias. Etch rates to 200 Å/min and 150 Å/min have been achieved with Cl_2/Ar and BCl_3/Ar plasmas, respectively. Parametric studies are currently underway to optimize etching parameters employing the Cl_2/Ar gas plasma.

14. SUBJECT TERMS

gallium nitride, GaN, aluminum nitride, AlN, $Al_xGa_{1-x}N$, organometallic vapor phase epitaxy, OMVPE, α(6H)-SiC(0001) substrates, doping, n-type, p-type, heterojunction, photoluminescence, PL, cathodoluminescence, CL, reactive ion etching, cracking cell

15. NUMBER OF PAGES

58

16. PRICE CODE

17. SECURITY CLASSIFICATION OF REPORT	18. SECURITY CLASSIFICATION OF THIS PAGE	19. SECURITY CLASSIFICATION OF ABSTRACT	20. LIMITATION OF ABSTRACT
UNCLAS	UNCLAS	UNCLAS	SAR

Table of Contents

I. Introduction

Continued development and commercialization of optoelectronic devices, including light-emitting diodes and semiconductor lasers produced from III–V gallium arsenide-based materials, has also generated interest in the much wider bandgap semiconductor mononitride materials containing aluminum, gallium, and indium. The majority of the studies have been conducted on pure gallium nitride thin films having the wurtzite structure, and this emphasis continues to the present day. Recent research has resulted in the fabrication of p–n junctions in wurtzitic gallium nitride, the deposition of cubic gallium nitride, as well as the fabrication of multilayer heterostructures and the formation of thin film solid solutions. Chemical vapor deposition (CVD) has usually been the technique of choice for thin film fabrication. However, more recently these materials have also been deposited by plasma-assisted CVD and reactive and ionized molecular beam epitaxy.

The program objectives achieved in this reporting period have been (1) the growth of undoped, high resistivity and n- and p-type doped monocrystalline, GaN thin films on α(6H)-SiC(0001) wafers via organometallic vapor phase epitaxy (OMVPE), and their characterization via photoluminescence (2) the growth and cathodoluminescence characterization of $Al_xGa_{1-x}N$ alloys and abrupt heterojunctions of these alloys, (3) the development and application of a novel NH_3 cracker cell for gas source MBE to reduce film damage and (4) the reactive ion etching of undoped GaN films via use of Cl-containing compounds.

The procedures, results, discussions of these results and conclusions of these studies are summarized in the following sections with reference to appropriate SDIO/ONR reports for details. Note that each major section is self-contained with its own figures, tables and references.

II. Undoped and Doped GaN and $Al_xGa_{1-x}N$ Thin Films Deposited on High-Temperature Monocrystalline AlN Buffer Layers on Vicinal and On-axis α(6H)-SiC(0001) Substrates via Organometallic Vapor Phase Epitaxy

M. D. Bremser, T. W. Weeks, Jr. and R. F. Davis

Abstract

Monocrystalline GaN(0001) thin films have been grown at 950°C on high-temperature, ≈100 nm thick, monocrystalline AlN(0001) buffer layers pre-deposited at 1100°C on α(6H)-$SiC(0001)_{Si}$ substrates via OMVPE in a cold-wall, vertical, pancake-style reactor. These films were free of low-angle grain boundaries and the associated oriented domain microstructure. The PL spectra of the GaN films deposited on both vicinal and on-axis substrates revealed strong bound excitonic emission with a FWHM value of 4 meV. This near band-edge emission from films on the vicinal substrates was shifted slightly to a lower energy, indicative of films containing residual tensile stresses. A peak attributed to free excitonic emission was also clearly observed in the on-axis spectrum. Undoped films were too resistive for accurate Hall-effect measurements. Controlled n-type, Si-doping in GaN was achieved for net carrier concentrations ranging from approximately 1×10^{17} cm^{-3} to 1×10^{20} cm^{-3}. Mg-doped, p-type GaN was achieved with $n_A - n_D \approx 3 \times 10^{17}$ cm^{-3}, $\rho \approx 7$ Ω·cm and $\mu \approx 3$ $cm^2/V \cdot s$ as measured by Hall-effect. Double-crystal x-ray rocking curve measurements for simultaneously deposited 1.4 μm GaN films revealed FWHM values of 58 and 151 arc sec for deposition on on-axis and off-axis 6H-$SiC(0001)_{Si}$ substrates, respectively. The corresponding FWHM values for the AlN buffer layers were approximately 200 and 400 arc sec, respectively.

$Al_xGa_{1-x}N$ films have been grown for $0 \leq x \leq 1$. Abrupt heterojunctions have been demonstrated in this system. Cathodoluminescence spectra of $Al_xGa_{1-x}N$ films for $x < 0.5$ showed intense near band-edge emission. Double-crystal x-ray rocking curve measurements revealed increasing FWHM values with increasing values of x. The FWHM values were smaller for AlGaN films grown on on-axis substrates than for simultaneously deposited films grown on vicinal substrates. As-deposited Si-doped $Al_{0.75}Ga_{0.25}N$ exhibited negative electron affinity.

*Portions of this report have been submitted as separate papers to *Applied Physics Letters* and the *Journal of Materials Research.*

A. Introduction

Recent research regarding II-VI compound semiconductors and device structures has culminated in the successful fabrication of the first blue-green[1] and blue[2] injection laser diodes (LDs) and high-efficiency blue[3] light emitting diodes (LEDs). Comparatively, the direct band gap III-V nitrides possess greater physical hardness, much larger heterojunction offsets, higher melting temperatures and higher thermal conductivities[4]. GaN (wurtzite structure), the most studied of the III-V nitrides, has a room temperature band gap of 3.39 eV and forms continuous solid solutions with both AlN (6.28 eV) and InN (1.95 eV). As such, materials with engineered band gaps are feasible for optoelectronic devices tunable in wavelength from the visible (600 nm) to the deep UV (200 nm). The relatively strong atomic bonding and wide band gaps of these materials also points to their potential use in high-power and high-temperature microelectronic devices. Specific applications for these wide band gap semiconductors include UV, blue and blue-green light emitting diodes, UV photodetectors, short-wavelength laser diodes and transit time limited microwave power amplifiers[5]. Concomitant with the realization and/or optimization of these devices is the present need for improved film quality.

Bulk single crystal wafers of AlN and GaN are not commercially available[6]. Sapphire(0001) is the most commonly used substrate, although its a-axis lattice parameter and coefficient of thermal expansion are significantly different from that of GaN (Table I). It was first observed by Yoshida *et al.*[7,8] that the electrical and luminescence properties of GaN films grown via reactive molecular beam epitaxy improved markedly when an AlN "buffer layer" was initially deposited on the sapphire(0001) substrate. Amano *et al.*[9,10] and Akasaki *et al.*[11]were the first to use an AlN buffer layer for improving GaN films deposited via organometallic vapor phase epitaxy (OMVPE). By decreasing the growth temperature of the AlN buffer layer from 1000°C to 600°C, further improvements in surface morphology, electrical measurements and luminescence properties of the GaN were observed[10,11]. At present, for OMVPE growth of GaN on sapphire(0001) substrates, the need for low-temperature (450°C-600°C) buffer layers of AlN[10-15] or GaN [13-16] appears paramount.

The growth process, transformations and resulting microstructures in the AlN and GaN films on sapphire(0001) substrates have been extensively investigated[10,11,14,15,17]. Specifically, the description given in Ref. 15 states that the low-temperature AlN is deposited as an amorphous film which undergoes solid phase epitaxy upon being annealed at the GaN growth temperature. The annealed AlN buffer layer has slightly misoriented (<3° in the basal plane[14]) columnar grains preferentially oriented along [0001] with a domain microstructure and associated low-angle boundaries. Subsequent GaN growth occurs by first nucleating on the individual AlN columns. These initial crystallites of the GaN epilayer reportedly undergo

Table I. Comparison of III-Nitride Material Properties with Various Substrate Materials.[a]

Material	Lattice Parameter at RT	Thermal Conductivity at RT	Coefficients of Thermal Expansion
2H-GaN	a = 3.189 Å c = 5.185 Å	1.3 W/cm·K[b]	5.59×10^{-6}/K 7.75×10^{-6}/K[b]
2H-AlN	a = 3.112 Å c = 4.982 Å	2.5 W/cm·K[b]	4.15×10^{-6}/K 5.27×10^{-6}/K
6H-SiC	a = 3.08 Å c = 15.12 Å	4.9 W/cm·K	4.2×10^{-6}/K 4.68×10^{-6}/K
α-sapphire	a = 4.758 Å c = 12.99 Å	0.5 W/cm·K	7.5×10^{-6}/K 8.5×10^{-6}/K
MgO	a = 4.216 Å		10.5×10^{-6}/K
ZnO	a = 3.252 Å c = 5.213 Å		2.9×10^{-6}/K 4.75×10^{-6}/K

[a] From *Landolt-Börnstein*, Vol. 17, edited by O. Madelung (Springer, New York, 1982)
[b] From *Properties of Group III Nitrides*, edited by J.H. Edgar (INSPEC, London, 1994).

geometric selection[18] via grain orientation competition until an oriented domain structure emerges. Subsequently, lateral growth and coalescence of GaN islands occurs resulting in uniform films having smooth surfaces. However, as a result of the slight misorientation in the annealed AlN buffer layers, low-angle grain boundaries persist in the GaN films[14]. A similar growth mode is proposed for GaN growth on low-temperature GaN buffer layers[13,19-21].

However, until ongoing crystal growth research leads to larger GaN crystals and more easily achieved homoepitaxial deposition, closely matched substrates, in terms of lattice parameters and coefficients of thermal expansion, are desirable. Candidate materials include MgO, ZnO and SiC[4]. Significant improvements in film quality have not been reported using MgO[22] and ZnO[23-25]. As with sapphire, these insulating substrates also prohibit the use of backside electrical contacts. However, commercially available conductive 6H-SiC(0001) substrates[26], which are more closely matched in both lattice parameter and coefficient of thermal expansion to AlN and GaN (Table I), show considerable promise[27,28].

In the present research, GaN thin films were deposited on monocrystalline high-temperature (HT) AlN buffer layers previously deposited on the Si- or C-polar planes of vicinal and on-axis 6H-SiC substrates. Likewise, AlN buffer layer growth was investigated on the various wafer types. The n- and p-type doping of GaN using Si and Mg dopants, respectively,

was also accomplished. However, since AlN has not been effectively doped n- or p-type, these insulating buffer layers prohibit front-and-backside electrical contacts, which are desirable for optoelectronic devices. As such, conductive $Al_xGa_{1-x}N$ buffer layers which do not compromise the resultant GaN film quality are sought.

B. Experimental Procedure

As-received vicinal and on-axis 6H-SiC$(0001)_{Si}$ and 6H-SiC$(000\bar{1})_C$ wafers[26] were cut into 7.1 mm squares. Vicinal 6H-SiC wafers were oriented 3°-4° off-axis toward the $<11\bar{2}0>$. These pieces were degreased in sequential ultrasonic baths of trichloroethylene, acetone and methanol and rinsed in deionized water. The SiC substrates were then dipped into a 10% HF solution for 10 minutes to remove the thermally grown oxide layer and blown dry with N_2 before being loaded onto a SiC-coated graphite susceptor contained in a cold-wall, vertical, pancake-style, OMVPE reactor. The system was evacuated to less than 3×10^{-5} Torr prior to initiating growth. The continuously rotating susceptor was RF inductively heated to the AlN deposition temperature of 1100°C or 1200°C (as measured optically on the susceptor) in 3 SLM of flowing H_2 diluent. Hydrogen was also used as the carrier gas for the various metalorganic reactants and dopants. Deposition of each AlN buffer layer was initiated by flowing triethylaluminum (TEA) and ammonia (NH_3) into the reactor at 23.6 μmol/min and 1.5 SLM, respectively. The system pressure during AlN growth was 45 Torr. Each AlN buffer layer was grown for 30 minutes resulting in a thickness of ≈100 nm. The TEA flow was subsequently terminated, the susceptor temperature decreased to 950°C and the system pressure increased to 90 Torr for the GaN growth. The flow rate of triethylgallium (TEG) was maintained at 24.8 μmol/min. The growth rate for GaN was ≈0.9 μm/hr. Silicon doped GaN films were grown by additionally flowing SiH_4 (8.2 ppm in balance of N_2) at flow rates between ≈0.05 nmol/min and ≈15 nmol/min. Magnesium doping was accomplished by introducing bis-cyclopentadienylmagnesium (Cp_2Mg) at a flow rate of 0.2 μmol/min.

Deposition of $Al_xGa_{1-x}N$ was initiated by flowing triethylaluminum (TEA) and triethylgallium (TEG) into the reactor at flow rates between 0 to 23.6 μmol/min and 0 to 24.8 μmol/min, respectively, corresponding to various alloy concentrations. TEA and TEG flow rates as a function of $Al_xGa_{1-x}N$ alloy composition are shown as a graph in Fig. 1.

Prior to being introduced into the reactor, the metalorganic precursors were fed into a gas mixing manifold, designed with a significantly reduce dead volume, to facilitate the deposition of abrupt heterojunctions. Ammonia (NH_3) flowing at 1.5 SLM was the source of nitrogen. The system pressure was 45 Torr. Silicon doping was accomplished by flowing silane (SiH_4) at 8.2 ppm in a balance of nitrogen into the reactor.

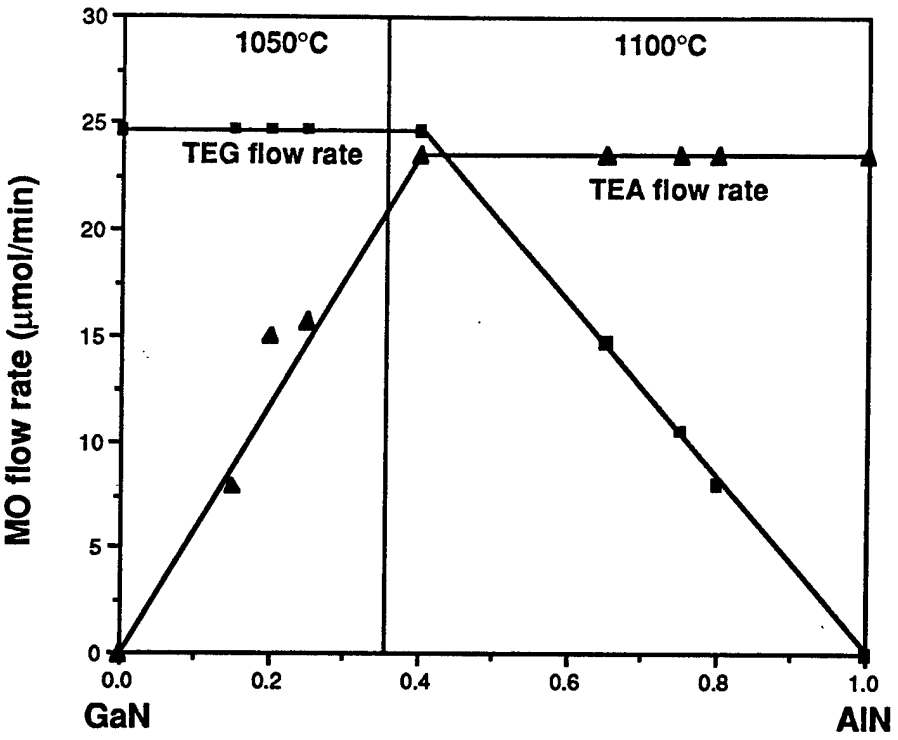

Figure 1. TEA and TEG flow rates as a function of $Al_xGa_{1-x}N$ alloy composition.

Four sets of undoped samples were examined on both vicinal and on-axis 6H-SiC(0001)$_{Si}$ and 6H-SiC(000$\bar{1}$)$_C$ substrates: (1) 1100°C AlN buffer layer, (2) 1200°C AlN buffer layer, (3) 950°C GaN on 1100°C AlN buffer layer and (4) 950°C GaN on 1200°C AlN buffer layer. Additionally, samples of $Al_xGa_{1-x}N$ for various compositions were grown on both vicinal and on-axis 6H-SiC(0001)$_{Si}$ and 6H-SiC(000$\bar{1}$)$_C$ substrates *without* a HT-AlN buffer layer.

The structural, microstructural, optical and electrical characteristics of the epitaxial GaN thin films were analyzed using several techniques. Scanning electron microscopy (SEM) was performed using a JEOL 6400FE operating at 5 kV. Conventional and high resolution transmission electron microscopy (TEM) were performed on a Topcon EM-002B microscope operating at 200 kV. Double-crystal x-ray rocking curve (DCXRC) measurements for the GaN(0004) and AlN(0002) reflections were made on a double-crystal diffractometer using Cu K_α. The $Al_xGa_{1-x}N$ alloy concentrations were determined using Auger Electron Spectrometry (AES). The photoluminescence (PL) properties of the GaN films were determined at 8K using a 15 mW He-Cd laser (λ = 325 nm) as the excitation source. The cathodoluminescence (CL) properties of the GaN films were determined at 8K using a Kimball Physics electron gun operating at 7 keV. NEA was investigated by ultraviolet photoemission spectroscopy (UPS) using a helium resonance lamp (the He I line) to provide a source of

21.2 eV light. Spectroscopic ellipsometry (SE) was performed in a dry nitrogen ambient on a rotating analyzer ellipsometer with an angle of incidence of 67.08° and equipped with a xenon arc lamp having a spectral range of 1.5eV-6 eV. The carrier concentrations and mobilities in the Si-doped GaN films were characterized by Hall-effect measurements (Van der Pauw geometry) using a modified Keithley Model 80 equipped with a sensitive digital voltmeter (Keithley Model 182DMM). Thermally evaporated Al served as the ohmic contacts to these films. Mg-doped GaN samples were tested using a Hg-probe C-V system (MDC CSM/2), a 4-point probe system (VEECO FPP-5000) and the above mentioned Hall system using thermally evaporated In contacts. Separately deposited AlN buffer layers were characterized via reflection high-energy electron diffraction (RHEED), SEM and DCXRC measurements.

C. Results and Discussion

High-Temperature AlN Buffer Layers. The surfaces of the 1100°C and 1200°C AlN buffer layers were mottled and textured with very small hillocks, respectively, on both the vicinal and on-axis 6H-SiC$(000\bar{1})_C$ wafers as observed via SEM. These growth templates yielded hexagonal hillocks, nominally 10 μm wide, on the surfaces of the subsequently grown GaN films. However, the AlN grown on the vicinal and on-axis 6H-SiC$(0001)_{Si}$ substrates had a smooth surface morphology. RHEED studies indicated that these films were monocrystalline as-deposited. In contrast, RHEED results indicated that AlN deposited on 6H-SiC$(0001)_{Si}$ substrates in the range of 500°C-1050°C resulted in polycrystalline material. Subsequent GaN deposition on these lower temperature buffer layers consisted essentially of the random nucleation and growth of isolated islands. The enhanced surface mobility of the adatoms at temperatures ≥1100°C and the relatively small mismatch in lattice parameters between AlN(0001) and 6H-SiC(0001) ($\Delta a/a_0 \approx 1\%$) promoted the growth of monocrystalline AlN(0001) films[27,28]. However, many small pits, nominally 30 nm in diameter, were observed on the AlN surfaces when using both Si-face wafer types. The pit density was decreased by increasing the AlN deposition temperature from 1100°C to 1200°C. This decrease was greater in on-axis than in off-axis films.

Initial Growth of GaN on HT-AlN. Coalescence of GaN islands occurred on monocrystalline HT-AlN buffer layers on vicinal and on-axis 6H-SiC$(0001)_{Si}$ substrates within the first several hundred angstroms of growth. The SEM image in Fig. 2 shows an intermediate stage of coalescence of ≈150Å thick GaN islands after one minute of growth.

After this initial coalescence, GaN growth occurred by a layer-by-layer mechanism. In contrast, for GaN film growth on low-temperature buffer layers on sapphire(0001), a similar growth scenario pertains but requires ≥30 minutes, several thousand angstroms of deposition and crystallographic geometric selection by the depositing atoms before island coalescence and layer-by-layer growth result[11,15].

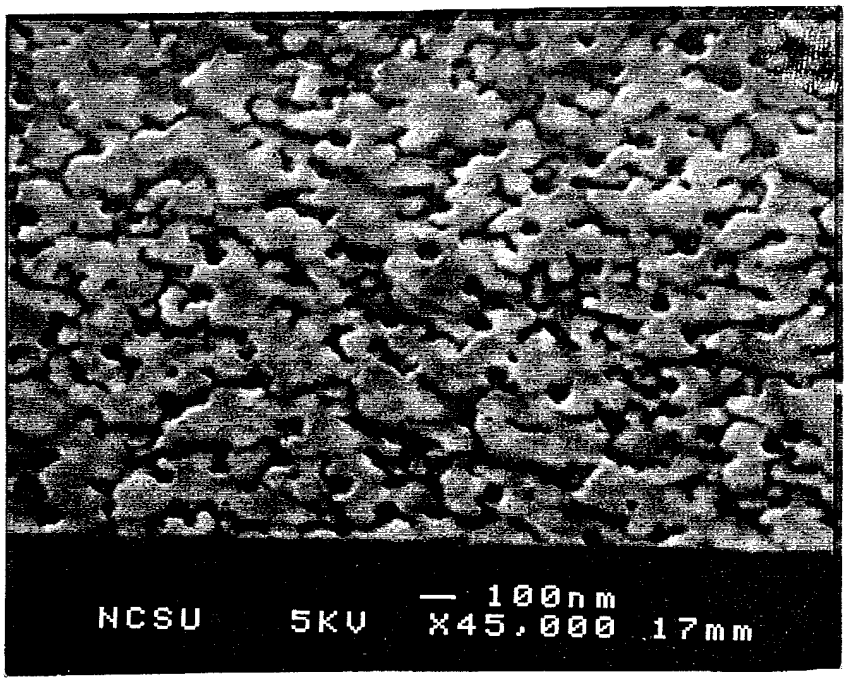

Figure 2. SEM image showing an intermediate stage of coalescence of ≈150Å thick GaN islands after 1 minute of growth on a monocrystalline AlN buffer layer deposited at 1100°C on a 6H-SiC(0001)$_{Si}$ substrate.

GaN Surface Morphology. The GaN films deposited on the HT-AlN buffer layers on the on-axis 6H-SiC(0001)$_{Si}$ substrates had very smooth surfaces as shown in Figs. 3(a) and 3(b).

Random pinholes, possibly caused by incomplete coalescence of the GaN, were observed on the otherwise featureless surface. A slightly mottled surface for GaN films grown on vicinal 6H-SiC(0001)$_{Si}$ substrates was observed in plan view SEM (Fig.4(a)), probably as a result of the higher density of steps coupled with the mismatch in the Si/C and Al/N bilayer stacking sequences at selected steps[29] on the growth surface of this substrate. However, only the surface steps were seen in the corresponding higher resolution cross-sectional TEM images, as shown by the representative micrograph in Fig. 4(b). For the vicinal and on-axis growth, there was no apparent difference in surface morphology between the GaN films deposited on the 1100°C and 1200°C AlN buffer layers.

TEM of GaN on HT-AlN. GaN films deposited directly on 6H-SiC(0001)$_{Si}$ substrates at 900°C and 45 Torr had columnar-like grains, faceted surfaces and high net carrier concentrations (n_D-$n_A > 1 \times 10^{19}$ cm^{-3}) [30]. In contrast, films deposited at 950°C on HT-AlN layers on similar 6H-SiC(0001)$_{Si}$ substrates were monocrystalline with no misorientation or low-angle grain boundaries, as determined via TEM by selected area diffraction and microstructural analysis. The stacking fault density was noticeably very low. These results are apparent in the cross-sectional TEM micrographs shown in Figs. 5(a) and 5(b) for on- and off-axis growth, respectively.

(a)

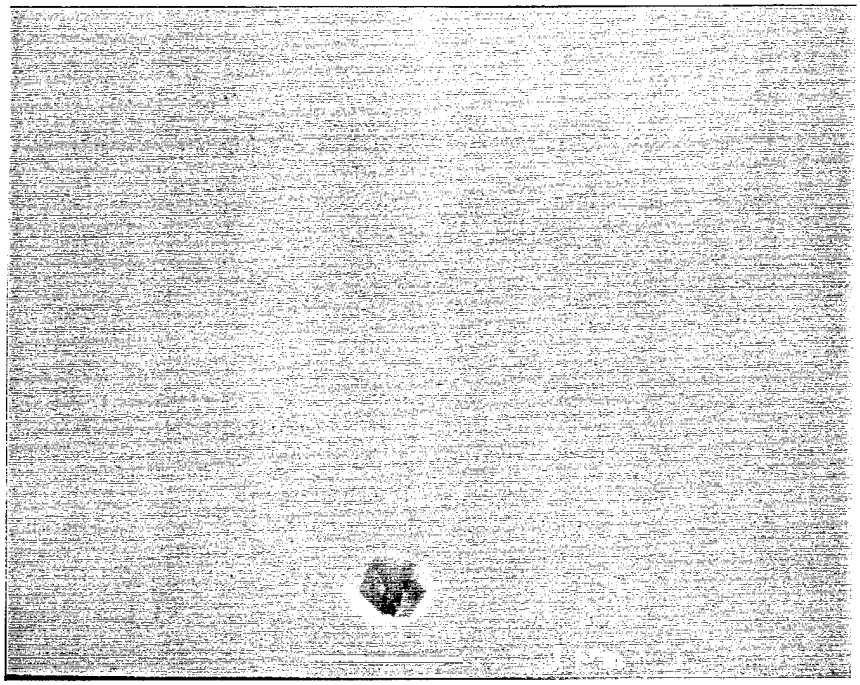

(b)

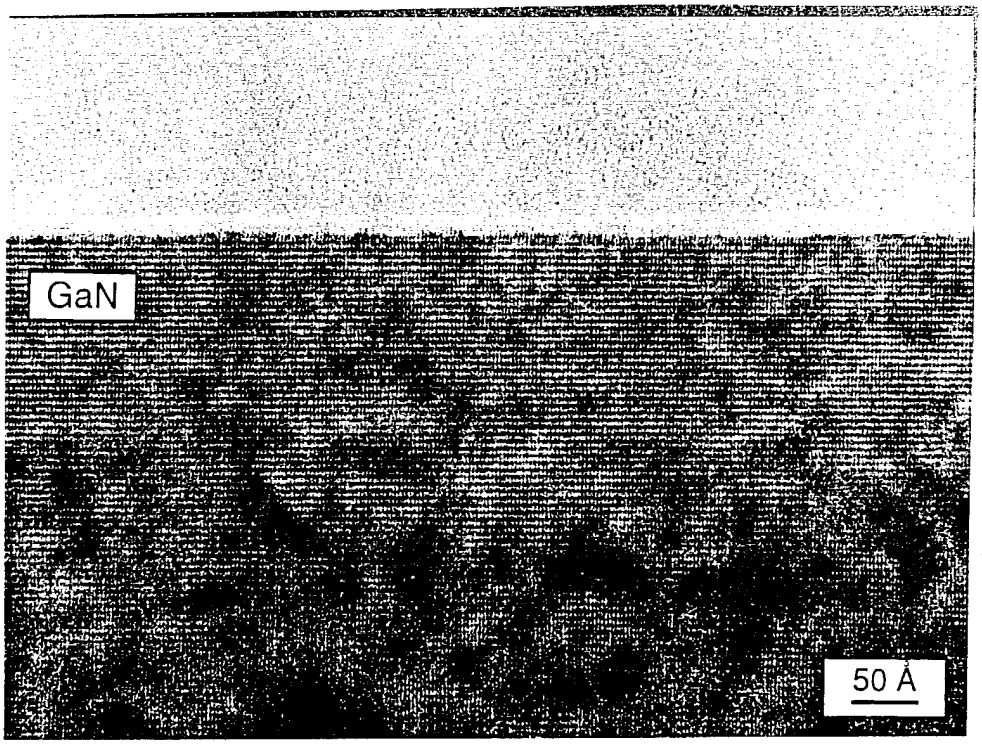

Figure 3. Plan view SEM (a) and cross-sectional TEM micrographs (b) of the surface of GaN deposited at 950°C on an AlN buffer layer grown at 1100°C on on-axis 6H-SiC(0001)$_{Si}$ substrates.

(a)

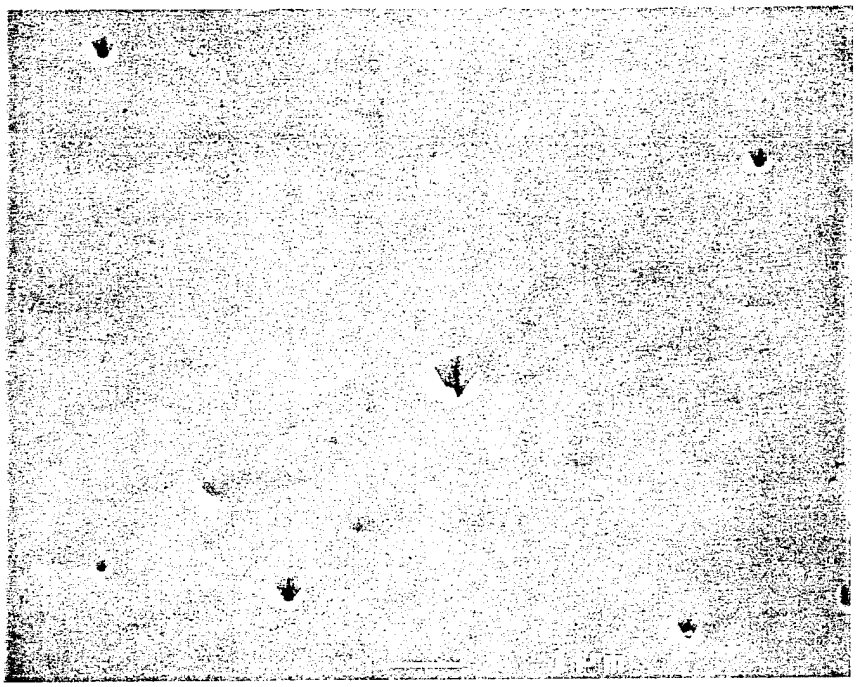

(b)

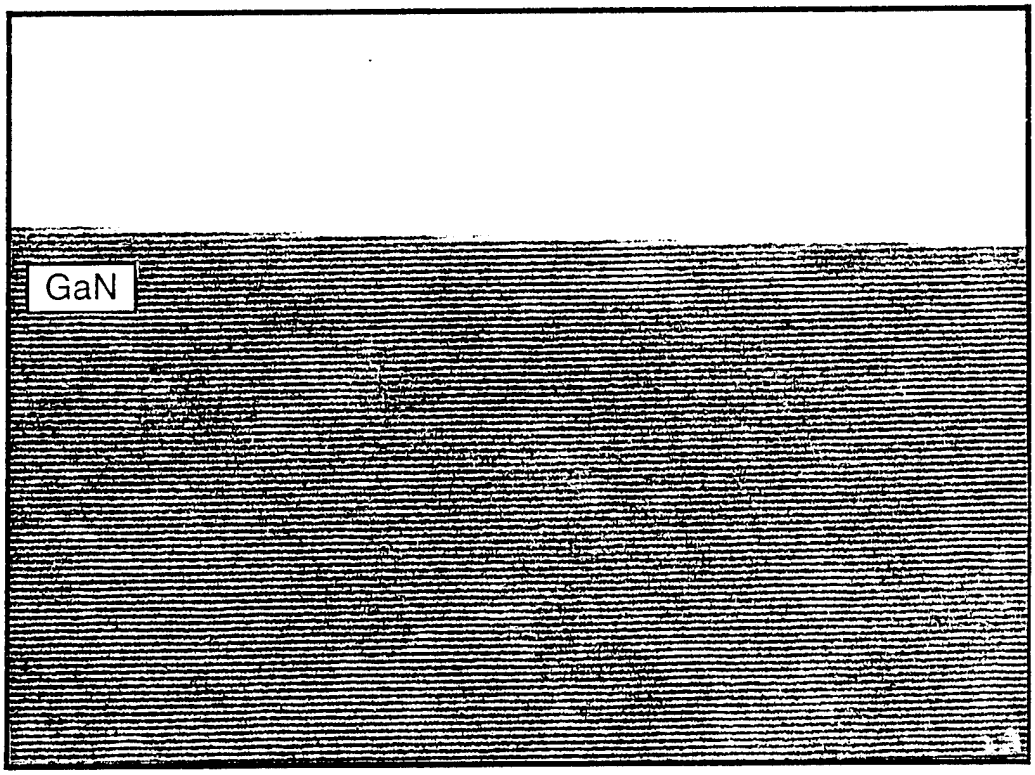

Figure 4. Plan view SEM (a) and cross-sectional TEM micrographs (b) of the surface of GaN deposited at 950°C on an AlN buffer layer grown at 1100°C on vicinal 6H-SiC(0001)$_{Si}$ substrates.

(a)

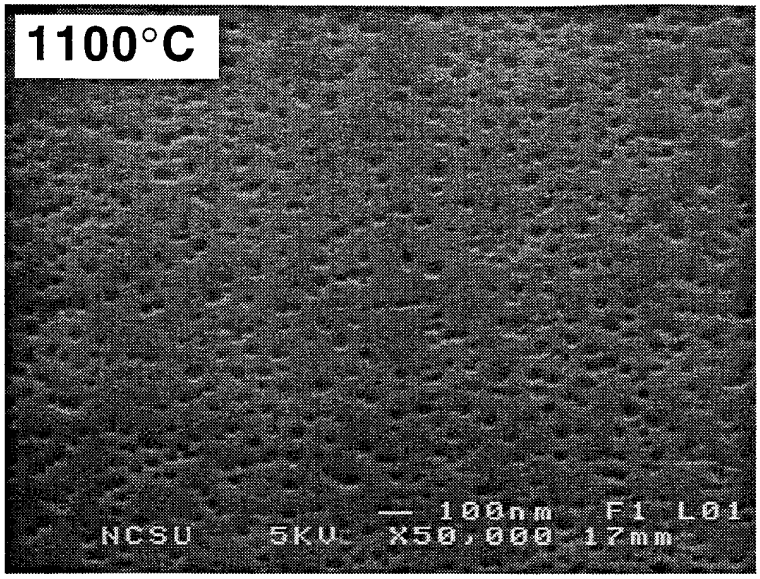

on-axis

(b)

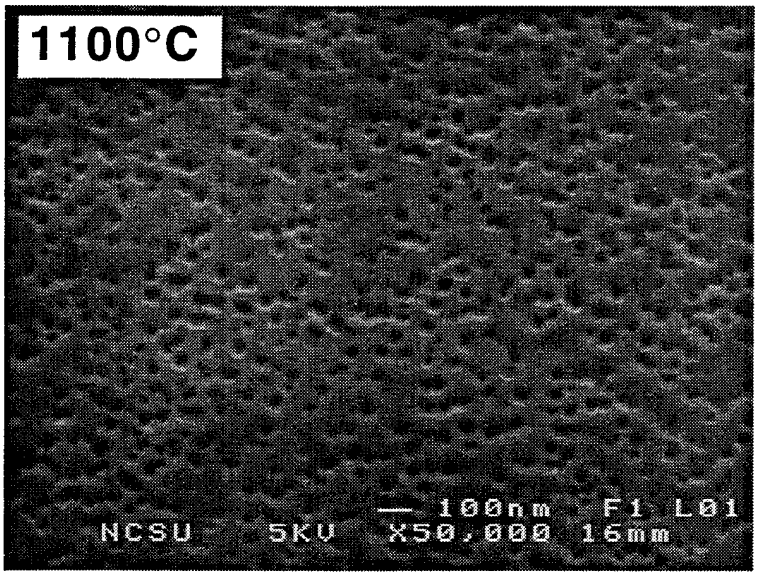

off-axis

Figure 5. Cross-sectional TEM micrographs of GaN grown at 950°C via OMVPE on a monocrystalline AlN buffer layer deposited at 1100°C on (a) on-axis and (b) vicinal 6H-SiC(0001)$_{Si}$ substrates.

Residual lattice strain resulting from double positioning boundaries (DPBs)[29], generated at the SiC steps as a result of the difference in the Si/C and Al/N bilayer stacking sequence along [0001], and resultant threading dislocations were apparent in the AlN buffer layers. The dislocation density within the first 0.5 μm of the GaN film on the vicinal 6H-SiC(0001)$_{Si}$

substrate was approximately 1×10^9 cm^{-2}, as determined from initial plan view TEM analysis by counting the number of dislocation per unit area. This value is approximately an order of magnitude lower than that reported[14] for thicker GaN films deposited on sapphire(0001) substrates using low-temperature buffer layers. As shown in Fig. 4(b), the dislocation density of the GaN film deposited on the vicinal 6H-SiC(0001)$_{Si}$ substrate decreased rapidly as a function of thickness. In contrast, since the on-axis wafers had less step and terrace features, the HT-AlN buffer layers on these substrates were of higher microstructural quality with smoother surfaces and fewer DPBs. Consequently, the microstructural quality of the GaN films and the AlN buffer layers were better for on-axis growth as shown by the DCXRC data noted below. As shown in Fig. 4, the dislocation density of the GaN film grown on-axis is comparable to the much thicker GaN film grown on the off-axis 6H-SiC(0001)$_{Si}$ substrate.

XRC Measurements. DCXRC measurements taken on simultaneously deposited 1.4 μm GaN films on HT-AlN (1100°C) buffer layers revealed FWHM values of 58 and 151 arc sec for deposition on the on-axis and off-axis 6H-SiC(0001)$_{Si}$ substrates, respectively. The FWHM values of the DCXRC values for the corresponding ≈100 nm AlN buffer layers were approximately 200 and 400 arc sec, respectively. These latter values were unchanged by increasing the growth temperature to 1200°C. The 2.7 μm GaN film deposited under identical conditions on a vicinal 6H-SiC(0001)$_{Si}$ substrate and shown in Fig. 5(b) yielded a FWHM value of 66 arc sec. The reduction in FWHM values from 151 to 66 arc sec is consistent with the decrease in the dislocation density as a function of thickness for GaN films grown on vicinal 6H-SiC(0001)$_{Si}$ substrates, as noted above. Likewise, the FWHM value (58 arc sec) of the thinner (1.4 μm) GaN film grown on-axis is comparable to the FWHM value (66 arc sec) of the thicker (2.7 μm) GaN film grown off-axis.

Photoluminescence and Spectroscopic Ellipsometry The low-temperature (8K) PL spectra (Fig. 6) of the simultaneously deposited 1.4 μm GaN films on the (a) on-axis and (b) vicinal 6H-SiC(0001)$_{Si}$ substrates showed strong near band-edge emission at 357.74 nm (3.466 eV) and 358.00 nm (3.463 eV), respectively (Fig. 7), which has been attributed to an exciton bound to a neutral donor[31].

The FWHM values of these I_2 bound exciton peaks were 4 meV. The near band-edge peak on the vicinal samples was significantly stronger than that from the on-axis films (see Fig. 6). Additionally, the spectrum of the material on the vicinal substrate was shifted to a slightly lower energy, indicative of the tensile stresses in the film. This finding was independently verified by SE[32]. A peak centered at 357.14 nm (3.472 eV) attributed to free excitonic emission was also clearly observed in the on-axis spectrum by PL. This free excitonic emission in the vicinal sample was dominated by the very intense I_2 peak. SE further resolves the A and B free excitons at room temperature for films grown on both vicinal and on-axis substrates.

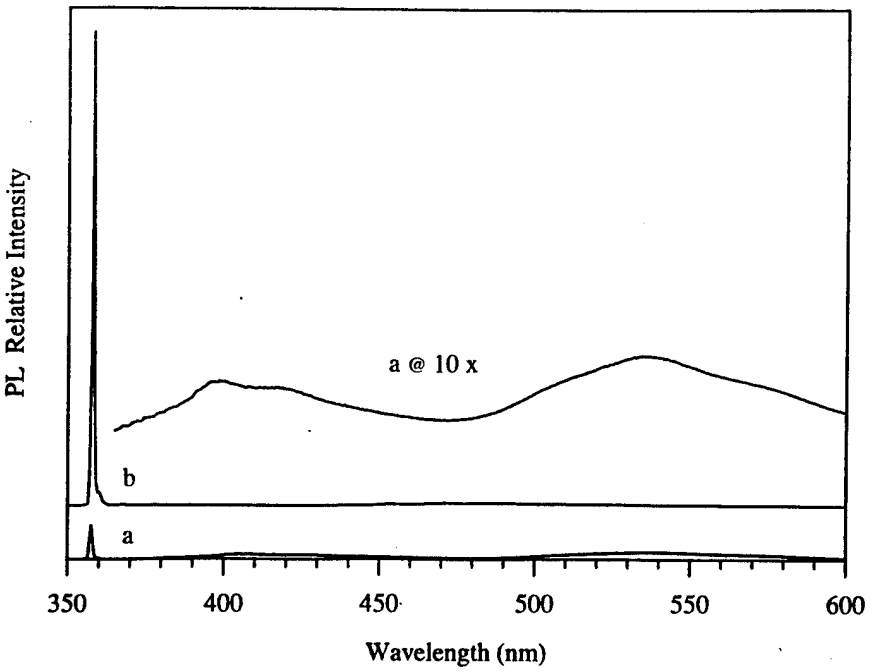

Figure 6. The low-temperature (8K) PL spectra of the GaN films on (a) on-axis and (b) vicinal 6H-SiC(0001)$_{Si}$ substrates. Inset shows details of the near band-edge region.

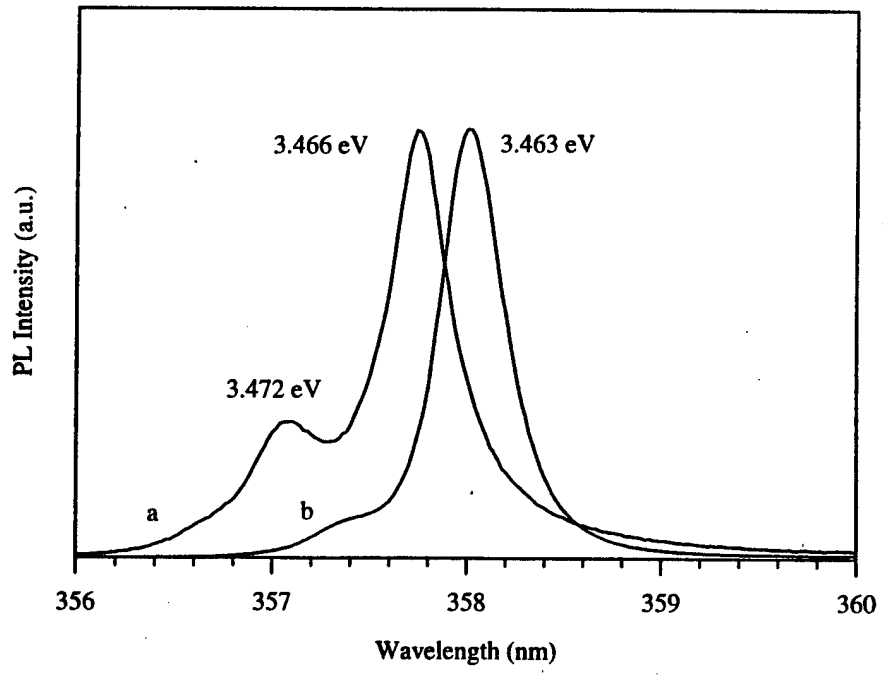

Figure 7. The low-temperature (8K) PL spectra of near bandedge emission of the GaN films on (a) on-axis and (b) vicinal 6H-SiC(0001)$_{Si}$ substrates.

Using SE, work is in progress to quantify both the hydrostatic and non-hydrostatic components of the residual strain in these films, as well as those grown on on-axis substrates[32]. The spectrum from the GaN film on the vicinal substrate revealed no observable emission at ≈545 nm (2.2 eV), commonly associated with deep-levels (DL) in the band gap[33]. A very weak 2.2 eV peak was observed in the GaN film grown on-axis. Similar variations in the PL spectra were also observed for GaN films grown on the vicinal and on-axis 6H-SiC$(000\bar{1})_C$ substrates. However, the peak associated with the free exciton was not clearly observed in the latter spectra. The causes of these PL spectral differences are under investigation.

Si-doping in GaN. Undoped high quality GaN films grown on HT-AlN buffer layers on both vicinal and on-axis 6H-SiC$(0001)_{Si}$ substrates were too resistive for Hall-effect measurements. Controlled n-type doping was achieved using SiH_4 for net carrier concentrations ranging from $\approx 1 \times 10^{17}$ cm^{-3} to $\approx 1 \times 10^{20}$ cm^{-3} in GaN films grown on vicinal 6H-SiC$(0001)_{Si}$ substrates. The net carrier concentrations and room temperature mobilities versus SiH_4 flow rate are plotted in Fig. 8. Films with a net carrier concentration of $n_D - n_A = 2 \times 10^{17}$cm^{-3} had a room temperature Hall mobility of $\mu = 375$ cm^2/V·s.

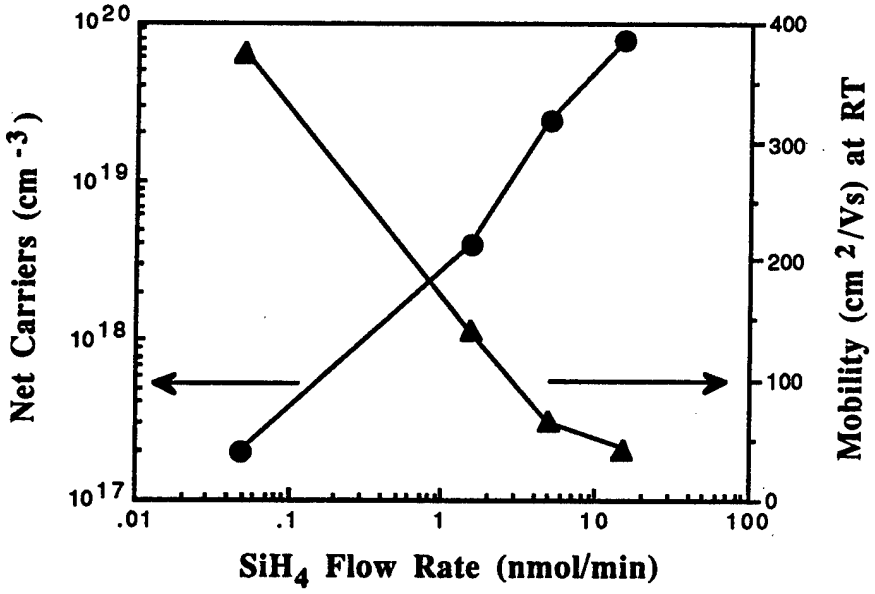

Figure 8. Net carrier concentration and room temperature mobilities in Si-doped, n-type GaN as a function of SiH_4 flow rate.

Mg-doping in GaN. Mg-doped GaN films were deposited at 950°C on HT-AlN (1100°C) buffer layers on vicinal 6H-SiC$(0001)_{Si}$ substrates by introducing Cp_2Mg at a flow rate of 0.2 μmol/min. These samples were subsequently annealed at 700°C at 700 Torr in 3 SLM of N_2 for 20 minutes. These same samples were re-annealed at 900°C for 20 minutes under

identical conditions. Figure 9 shows the PL (8K) spectra of the unannealed, 700°C annealed and 900°C annealed samples.

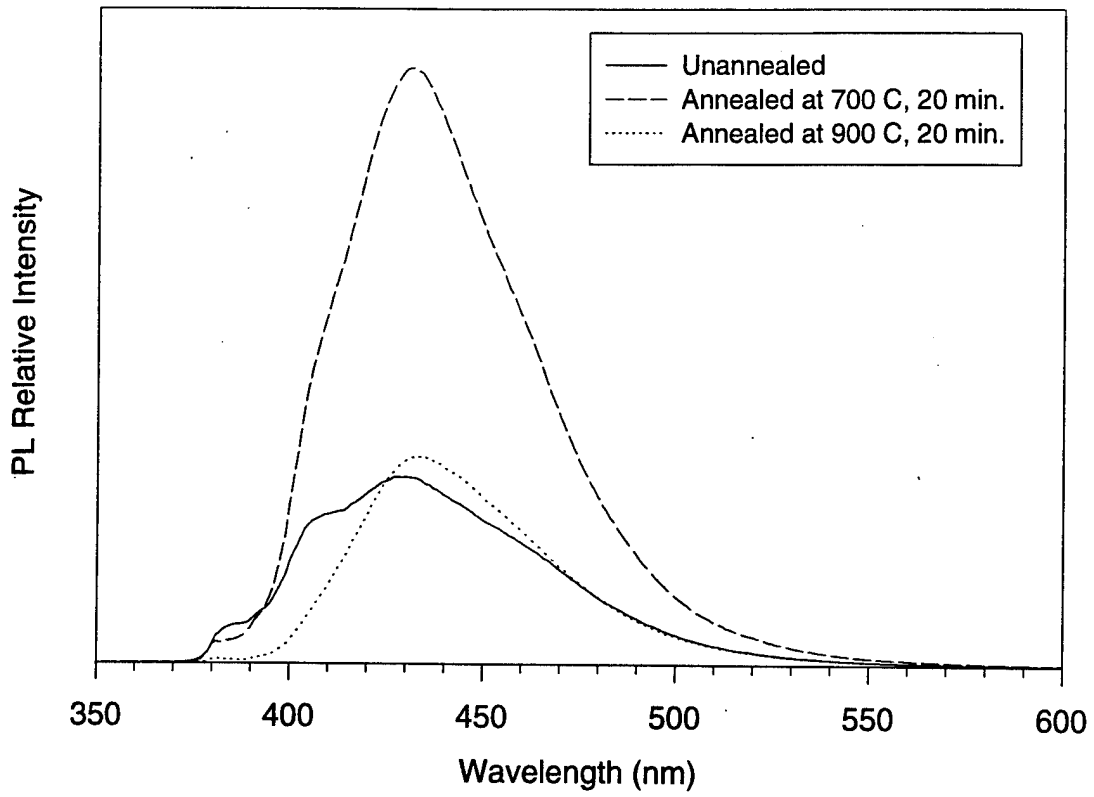

Figure 9. Low-temperature (8K) PL spectra of an unannealed, 700°C annealed and 900°C annealed Mg-doped GaN film.

Similar to the results of Nakamura *et al.*[34], the PL intensity of the blue emission was increased by the 700°C anneal and was dramatically decreased by the subsequent 900°C anneal. Hall-effect measurements made on the annealed samples revealed p-type GaN with a net hole carrier concentration of n_A-$n_D \approx 3 \times 10^{17}cm^{-3}$, a resistivity of $\rho \approx 7\ \Omega$·cm and a hole mobility of $\mu \approx 3\ cm^2/V{\cdot}s$. Likewise, 4-point probe and Hg-probe C-V measurements verified p-type GaN.

Additionally, Mg-doped GaN films were deposited at 1100°C on HT-AlN (1100°C) buffer layers on vicinal 6H-SiC(0001)$_{Si}$ substrates by introducing Cp_2Mg at a flow rate of 0.2 μmol/min. C-V measurements revealed p-type GaN *as-deposited* with n_A-$n_D \approx 2 \times 10^{16}cm^{-3}$. These samples were subsequently annealed at 600°C at 700 Torr in 3 SLM of N_2 for 20 minutes. The PL intensity of the blue emission was found to be the most intense after annealing at 600°C. P-type GaN with n_A-$n_D \approx 1 \times 10^{18}cm^{-3}$ was revealed by C-V measurements of the annealed films.

$Al_xGa_{1-x}N$ Film Growth. As shown in Fig. 1, $Al_xGa_{1-x}N$ films have been grown for Al mole fractions of $0 \leq x \leq 1$. The alloy concentrations were determined via AES by depth profiling through multi-layer heterostructures, one of which is shown in Fig. 10.

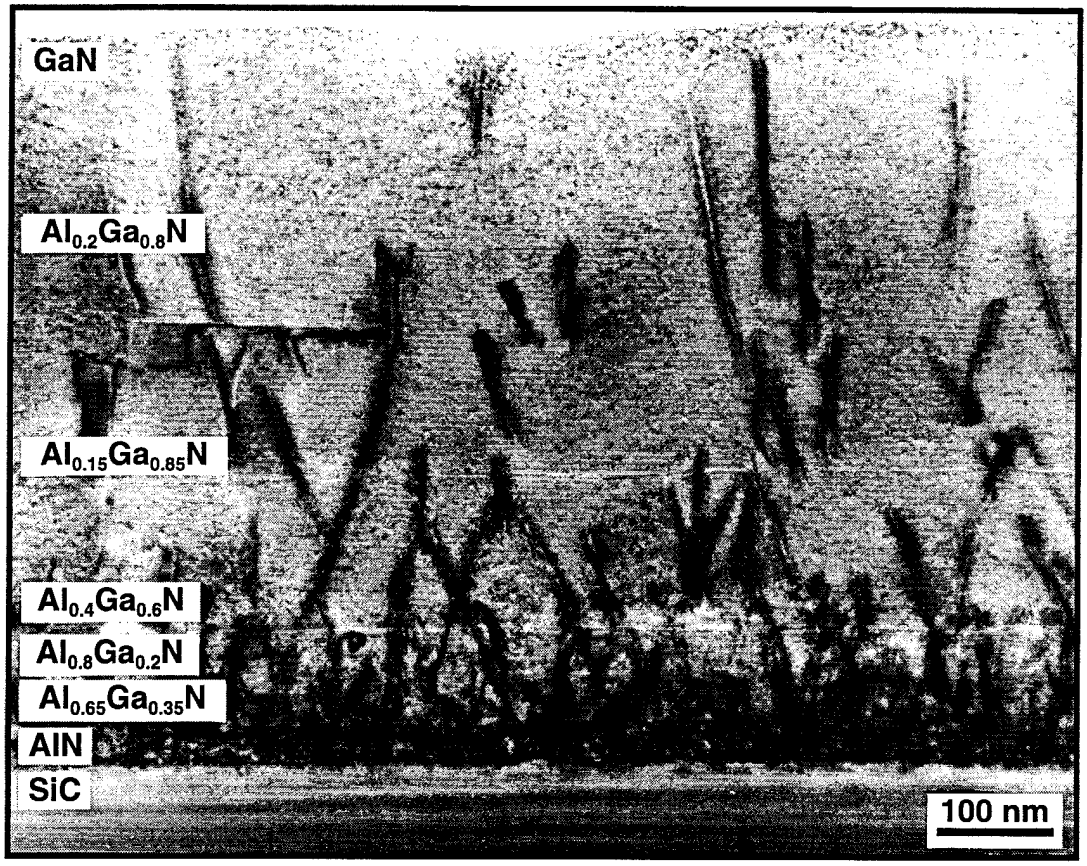

Figure 10. Cross-section TEM micrograph of a 7-layer $Al_xGa_{1-x}N$ heterostructure.

GaN and AlN served as the necessary standards. $Al_xGa_{1-x}N$ films for $0 < x < 0.3$ were then simultaneously deposited directly on vicinal and on-axis 6H-SiC(0001) substrates *without* the use of the customary high-temperature AlN buffer layers[28]. These films were electrically insulating as-grown. As shown in Fig. 11, SEM revealed a smooth surface for a 0.8 μm thick $Al_{0.12}Ga_{0.88}N$ film deposited directly on an on-axis substrate.

The Al mole fractions were determined by low-temperature CL measurements as described below. Similar to findings for GaN film growth[28], the DCXRC measurements revealed smaller FWHM values for AlGaN films grown on on-axis substrates as compared to simultaneously deposited films grown on vicinal substrates. Also, the FWHM values expand with increasing Al mole fraction. These results are shown in Fig. 12 where FWHM values are plotted versus alloy concentration for $Al_xGa_{1-x}N$ films simultaneously deposited on vicinal and on-axis 6H-SiC(0001) substrates.

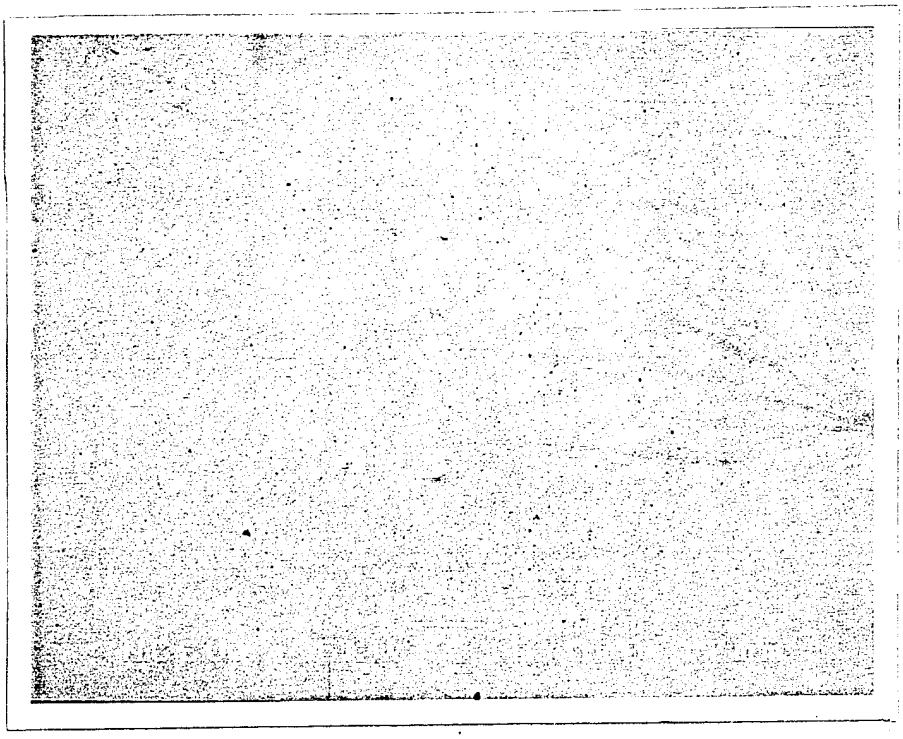

Figure 11. Plan-view SEM of a 0.8 micron thick $Al_{0.12}Ga_{0.88}N$ film deposited directly on an on-axis substrate.

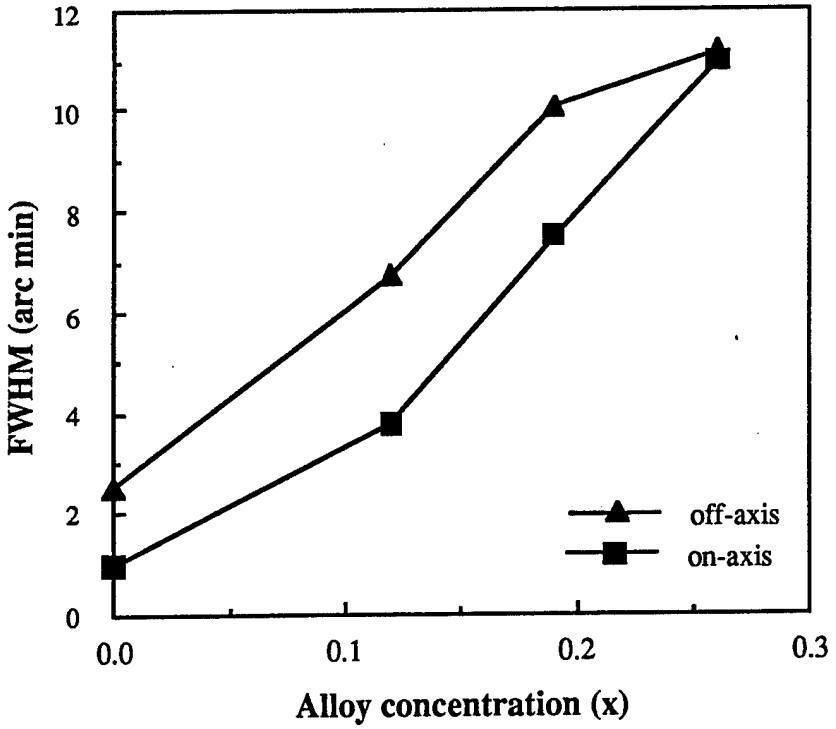

Figure 12. DCXRC FWHM values versus alloy concentration for $Al_xGa_{1-x}N$ films simultaneously deposited on vicinal and on-axis 6H-SiC(0001) substrates.

CL of $Al_xGa_{1-x}N$. The low-temperature (8K) CL spectra of the $Al_xGa_{1-x}N$ films with $x < 0.5$ showed strong near band-edge emission. Films with $x \geq 0.5$ are currently being investigated. As expected, the energy positions of these peaks shifted towards higher energy with increasing x, as shown in Fig. 13.

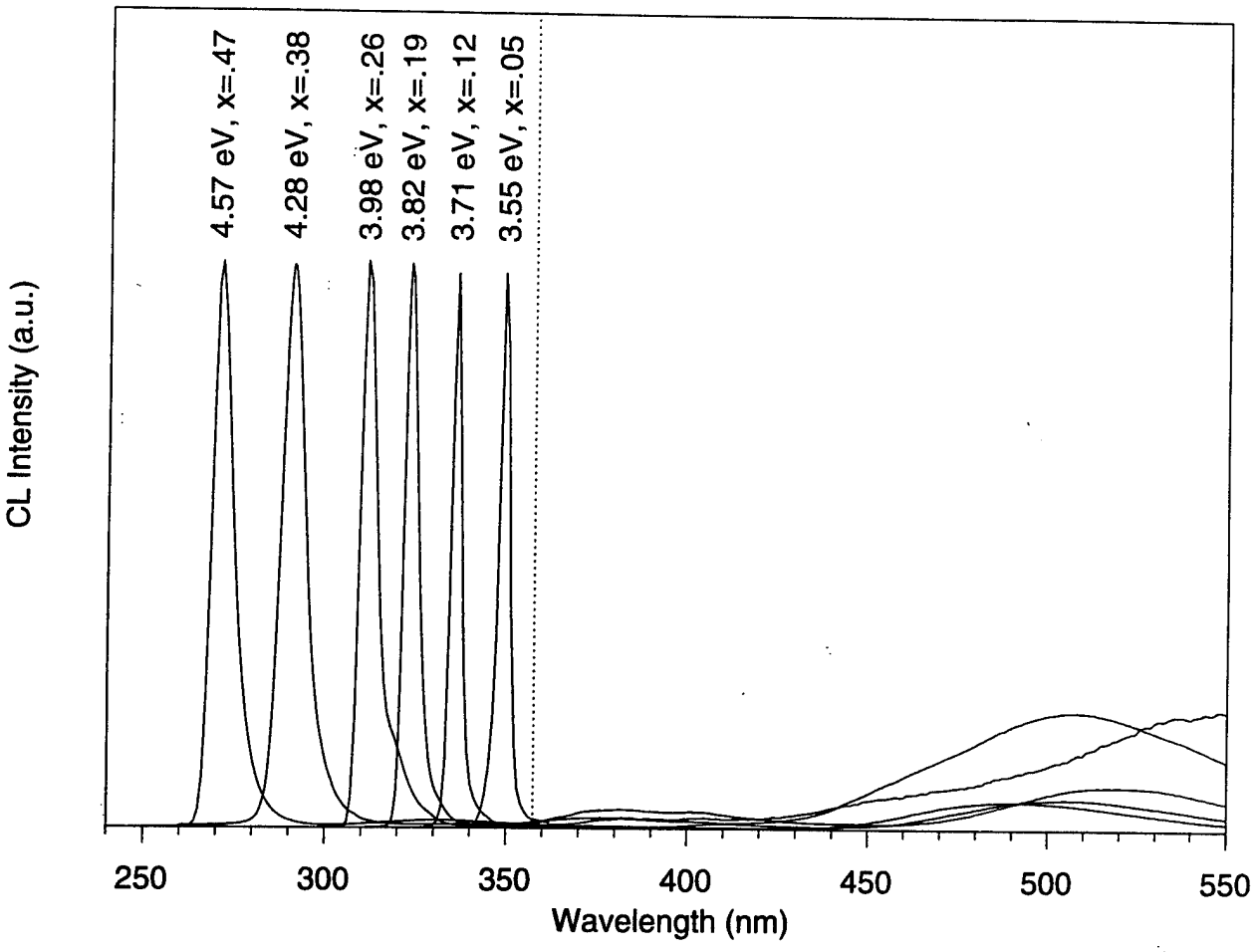

Figure 13. Low-temperature (8K) CL of $Al_xGa_{1-x}N$ films with $x < 0.5$.

The dashed line in the graph shows the peak position for $Al_xGa_{1-x}N$ where $x = 0$. Al mole fractions were assigned from the near band-edge peak positions using a bowing parameter of $b = 0.98$ eV, as determined by Khan *et al* [35]. Apparent in Fig. 14 is the increased FWHM values of the energy peaks with increasing values of x. Thus, Fig. 14 graphs the increasing FWHM values of these near band-edge peaks for undoped $Al_xGa_{1-x}N$ films grown on vicinal 6H-SiC(0001) substrates.

AlGaN films grown on on-axis substrates showed a similar trend. The broadening of the near band-edge peak is possibly due to increased fluctuations in the alloy compositions of $Al_xGa_{1-x}N$ films for increasing values of x [35]. Also, the CL peak intensities were 0.1 to 1

order of magnitude stronger for undoped AlGaN films grown on vicinal substrates than for films grown on on-axis substrates. This phenomenon is being investigated further.

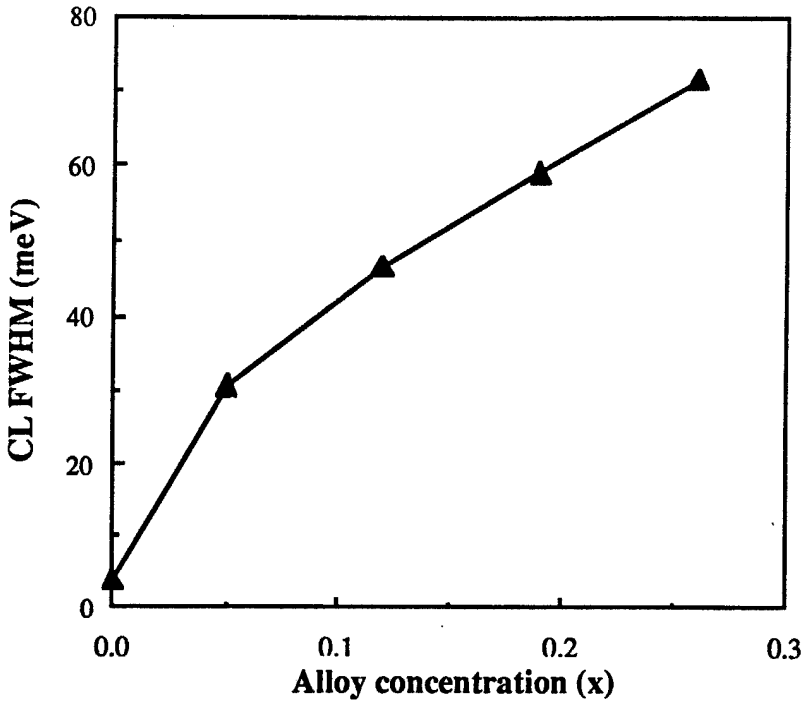

Figure 14. FWHM values of the CL near band-edge peak from $Al_xGa_{1-x}N$ films grown on vicinal 6H-SiC(0001) substrates.

Heterostructures of $Al_xGa_{1-x}N$. For the successful fabrication of super-lattices and multiple quantum well structures, abrupt heterojunctions are important. Thus, as shown in the cross-section SEM micrograph of Fig. 15, a multi-layer heterostructure was grown. The cross-sectional TEM image of this structure is shown in Fig. 16.

Including the initial AlN buffer layer, five distinct layers are observable. Therefore, using the reduced dead volume gas mixing manifold, abrupt heterojunctions were fabricated, similar to the AlN/GaN interface shown in Fig. 17.

Negative Electron Affinity in Si -doped $Al_{0.75}Ga_{0.25}N$. A Si-doped $Al_{0.75}Ga_{0.25}N$ film grown directly on vicinal 6H-SiC(0001) exhibited a NEA effect in the as-deposited state as determined by UPS. Because charging problems with insulating AlGaN can quickly quench the photoemission, the film was intentional Si-doped to minimize this effect. Figure 18 shows the UV photoemission of this sample exhibiting a distinctive peak indicative of the presence of NEA. A large sample bias (3 V) was needed to overcome the work function of the electron analyzer. Thus, the work function of $Al_{0.75}Ga_{0.25}N$ is apparently less than that of the analyzer, which is between 4 and 5 eV. Subsequent vacuum annealings at 475°C and 580°C quenched the NEA.

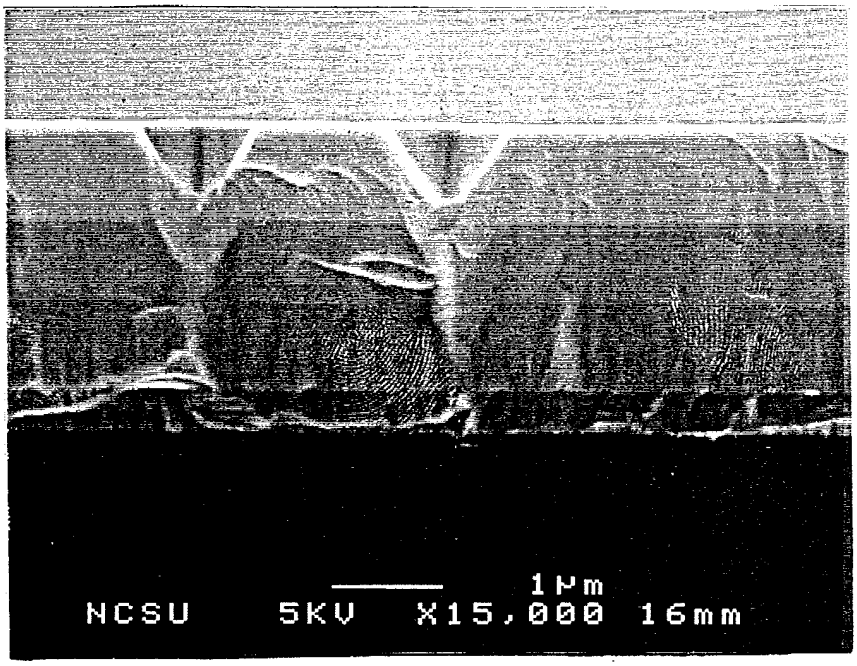

Figure 15. Cross-section SEM micrograph of a 5-layer heterostructure.

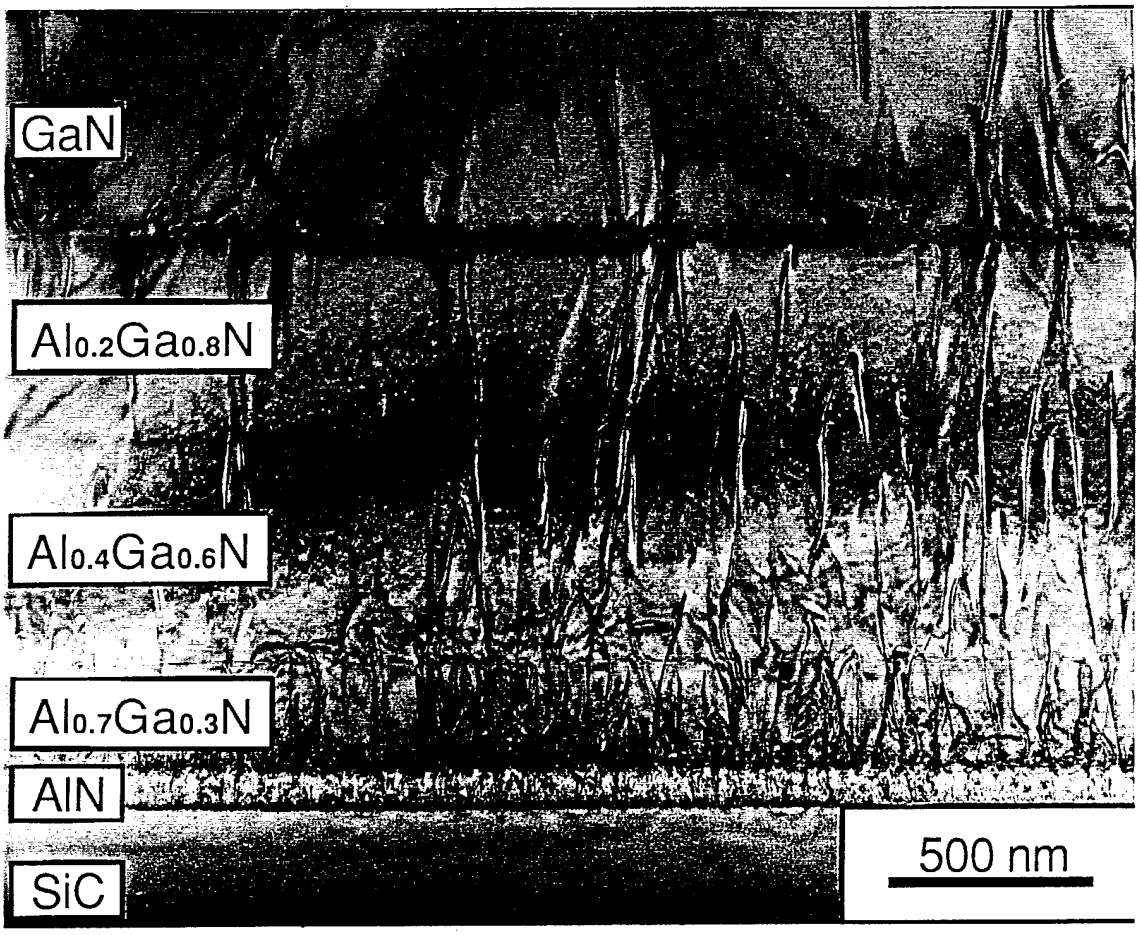

Figure 16. Cross-sectional TEM image of the heterostructure shown in Fig. 15.

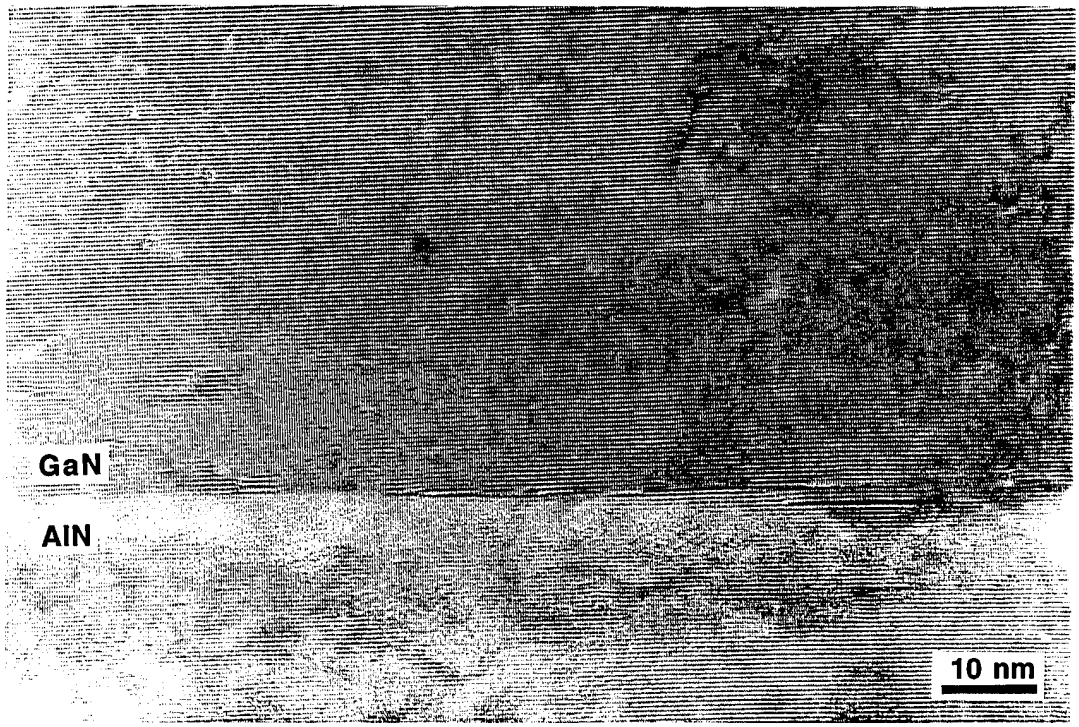

Figure 17. TEM micrograph showing the abruptness of an AlN/GaN interface.

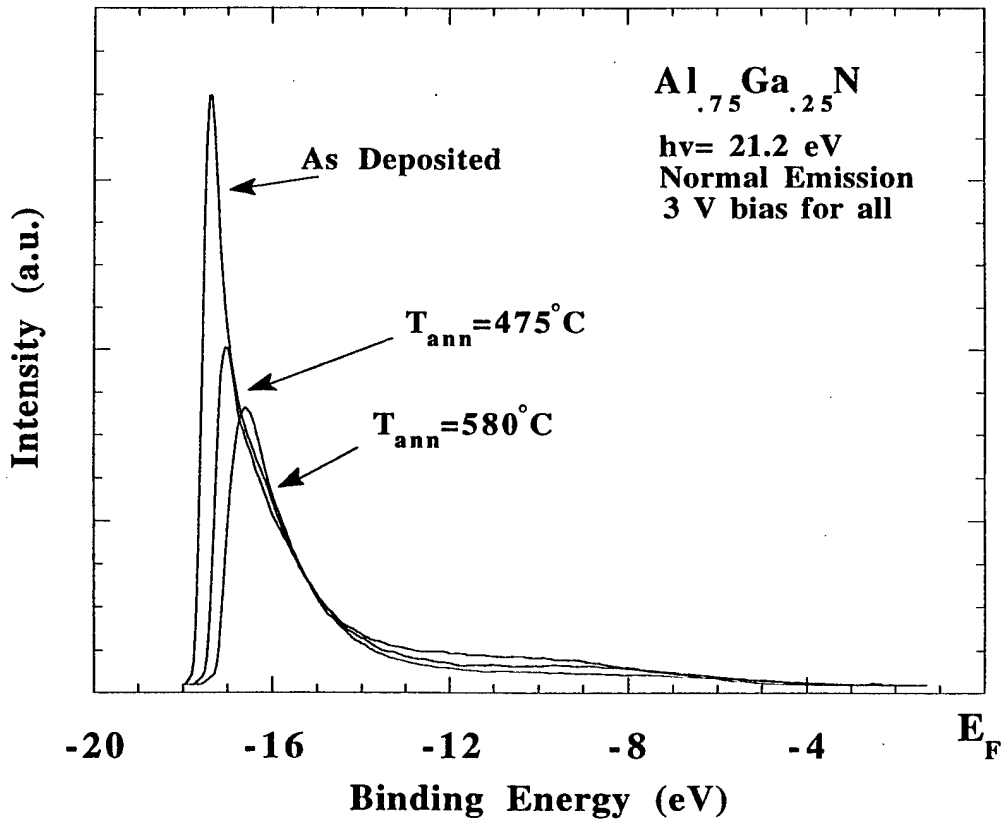

Figure 18. UV photoemission of $Al_{0.75}Ga_{0.25}N$ on 6H-SiC(0001) with a sample bias of 3 V. UPS spectra for the as-deposited state and subsequent anneals at 475°C and 580°C are shown.

D. Conclusions

GaN(0001) thin films void of low-angle grain boundaries and associated oriented domain microstructures have been grown at 950°C via OMVPE on monocrystalline AlN(0001) buffer layers previously deposited at 1100°C on vicinal and on-axis α(6H)-SiC(0001)$_{Si}$ substrates. The improved GaN film quality is a direct result of the achievement of monocrystalline HT-AlN buffer layers with no misorientations or low-angle grain boundaries. The GaN films grown on the vicinal substrates contained both a higher density of dislocations in the interface region and a higher residual stress. The latter was manifest in both a broader DCXRC FWHM value and a shift in the PL spectrum. Controlled n-type Si-doping of GaN was demonstrated for net carrier concentrations ranging from approximately 1×10^{17} cm^{-3} to 1×10^{20} cm^{-3}. Mg-doped p-type GaN was obtained as-deposited and upon annealing, n_A-n_D as high as 1×10^{18} cm^{-3} was achieved. For simultaneously deposited 1.4 μm films, DCXRC measurements for the GaN(0004) reflection indicated FWHM values of 58 and 151 arc sec for films grown on on-axis and off-axis 6H-SiC(0001)$_{Si}$ substrates, respectively. The corresponding FWHM values of the AlN(0002) reflection for the ≈100 nm buffer layers were approximately 200 and 400 arc sec, respectively. Each low-temperature (8K) PL spectrum of the GaN films deposited on both on-axis and vicinal substrates showed a strong bound exciton peak having a FWHM value of 4 meV. The spectrum of the material on the vicinal substrates was shifted to a lower energy, indicative of the tensile stresses in the film. The on-axis spectrum also contained a peak believed to be associated with free excitonic emission.

$Al_xGa_{1-x}N$ films have been grown for $0 \leq x \leq 1$. Abrupt heterojunctions have been demonstrated in this system. DCXRC measurements revealed smaller FWHM values for AlGaN films grown on on-axis 6H-SiC(0001) substrates as compared to simultaneously deposited films grown on vicinal substrates. Also, the FWHM values increase with increasing values of x. The CL spectra of the $Al_xGa_{1-x}N$ films for $x < 0.5$ showed strong near band-edge emission. FWHM values of the main energy peak increased with increasing Al mole fraction. Si-doped $Al_{0.75}Ga_{0.25}N$ exhibited a NEA effect in the as-deposited state.

E. Future Research Plans and Goals

With the achievement of both p- and n-type GaN, the fabrication of p-n homojunctions is possible, but mesa isolation of these junctions is needed for electrical testing. Further work will be undertaken to increase the maximum achievable net carrier concentration in p-type GaN. By demonstrating the growth of high quality $Al_xGa_{1-x}N$ films for $x < 0.3$ directly on 6H-SiC, doping of these films will allow for their use as a conducting buffer layer. Additionally, the growth of high quality $Al_xGa_{1-x}N$ for $x > 0.3$ is needed. Also, the electrical characterization of p- and n-type doping of $Al_xGa_{1-x}N$ must demonstrated. This will allow for the fabrication of single and double heterostructures for ultraviolet LEDs, photodetectors, and laser diodes.

These efforts will require the ability to grow thin quantum well structures. Concurrently, microelectronic devices such as MESFETs, MISFETs, and HBTs can be demonstrated. Ultimately, to be able to achieve these devices, preparation of the nitride surfaces which are free of post-deposition overlayers must achieved. By using spectroscopic ellipsometry in concert with other analytical techniques, this can be accomplished.

F. References

1. M. A. Haase, J. Qui, J. M. DePuydt and H. Cheng, Appl. Phys. Lett. **59**, 1272 (1991).
2. H. Jeon, J. Ding, A. V. Nurmikko, W. Xie, D. C. Grillo, M. Kobayashi, R. L. Gunshor, G. C. Hua and N.Otsuka, Appl. Phys. Lett. **60**, 2045 (1992).
3. W. Xie, D. C. Grillo, R. L. Gunshor, M. Kobayashi, H. Jeon, J. Ding, A. V. Nurmikko, G. C. Hua and N. Otsuka, Appl. Phys. Lett. **60**, 1999 (1992).
4. S. Strite and H. Morkoc, J. Vac. Sci. Technol. **B 10**, 1237 (1992).
5. M. Gershenzon, D. E. Wang, L. Ta, in *Proceedings 1981 International Optoelectronics Workshop, Tainan, Taiwan, December 1981*, edited by D. Y. Chang (National Cheng Kung University, Tainan, Taiwan) p. 139.
6. R. F. Davis, Physica B **185**, (1993).
7. S. Yoshida, S. Misawa and S. Gonda, Appl. Phys. Lett. **42**, 427 (1983).
8. S. Yoshida, S. Misawa and S. Gonda, J. Vac. Sci. & Technol. **B 1**, 250 (1983).
9. H. Amano, N. Sawaki, I. Akasaki and Y. Toyoda, Appl. Phys. Lett. **48**, 353 (1986).
10. H. Amano, I. Akasaki, K. Hiramatsu, N. Koide and N. Sawaki, Thin Solid Films **163**, 415 (1988).
11. I. Akasaki, H. Amano, Y. Koide, K. Hiramatsu and N. Sawaki, J. Cryst. Growth **98**, 209 (1989).
12. M. A. Khan, J. N. Kuznia, D. T. Olson and R. Kaplan, J. Appl. Phys. **73**, 3108 (1993).
13. J. N. Kuznia, M. A. Khan, D. T. Olson, R. Kaplan and J. Freitas, J. Appl. Phys. **73**, 4700 (1993).
14. W. Qian, M. Skowronski, M. De Graef, K. Doverspike, L. B. Rowland and D. K. Gaskill, Appl. Phys. Lett. **66**, 1252 (1995).
15. K. Hiramatsu, S. Itoh, H. Amano, I. Akaski, N. Kuwano, T. Shiraishi and K. Oki, J. Crystal Growth, **115**, 628 (1991) .
16. S. Nakamura, Jpn. J. Appl. Phys., **30**, L1705 (1991).
17. N. Kuwano, T. Shiraishi, A. Koga, K. Oki, K. Hiramatsu, H. Amano, K. Itoh and I. Akasaki, J. Cryst. Growth, **115**, 381 (1991) .
18. A. A. Chernov, Modern Crystallography III: Crystall Growth (Springer, Berlin, 1984) p. 283.
19. S. Nakamura, Jpn. J. Appl. Phys., **30**, 1620 (1991).
20. A. E. Wickenden, D. K. Wickenden and T. J. Kistenmacher, J. Appl. Phys., **75**, 5367 (1994).
21. D. K. Wickenden, J. A. Miragliotta, W. A. Bryden and T. J. Kistenmacher, J. Appl. Phys. **75**, 7585 (1994).
22. R. C. Powell, G. A. Tomasch, Y.-W. Kim, J. A. Thornton and J. E. Greene, Mater. Res. Soc. Symp. Proc. **162**, 525 (1990).
23. P. J. Born and D. S. Robertson, J. Mater. Sci. **15**, 30003 (1980).
24. K. Matsubara and T. Takagi, Jpn. J. Appl. Phys. **22**, 511 (1982).
25. Z. Sitar, M. J. Paisley, B. Yan and R. F. Davis, Mater. Res. Soc. Symp. Proc., **162**, 537 (1990).
26. Cree Research, Inc., 2810 Meridian Parkway, Suite 176, Durham, NC 27713
27. T. W. Weeks, Jr., M. D. Bremser, K. S. Ailey, E. Carlson, W. G. Perry and R. F. Davis (unpublished).

28. T. W. Weeks, Jr., M. D. Bremser, K. S. Ailey, E. Carlson, W. G. Perry, L. L. Smith, J. A. Freitas, Jr., R. F. Davis, Second Nitride Workshop, St. Louis, MO, October 17-18, 1994.
29. S. Tanaka, R. S. Kern and R. F. Davis, Appl. Phys. Lett. **66**, 37 (1995).
30. T. W. Weeks, Jr., D. W. Kum, E. Carlson, W. G. Perry, K. S. Ailey and R. F. Davis, Second International High Temperature Electronics Conference, Charlotte, NC, June 5-10, 1994.
31. R. Dingle, D. D. Sell, S. E. Stokowski and M. Ilegems, Phys. Rev. B **4**, 1211 (1971).
32. N. V. Edwards, T. W. Weeks, Jr., M. D. Bremser, H. Liu, R. A. Stall, R. F. Davis and D. E. Aspnes, Materials Research Society Spring Meeting, San Francisco, CA, April 17-20, 1995.
33. W. Götz, N. M. Johnson, R. A. Street, H. Amano and I. Akasaki, Appl. Phys. Lett. **66**, 1340 (1995).
34. S. Nakamura, T. Mukai, M. Senoh and N. Iwasa, Jpn. J. Appl. Phys. **31**, L139 (1992).
35. M. R. H. Khan, Y. Koide, H. Itoh, N. Sawaki and I. Akasaki, Solid State Commun. **60**, 509 (1986).

III. The Use of NH_2 for Film Growth

A. Introduction

AlN, GaN and InN thin films are presently grown by various techniques including MOVPE, RF sputtering, and electron cyclotron resonance (ECR) plasma assisted GSMBE. We are continuing to use the last technique to determine the optimal growth parameters for the binary compounds, selected solid solutions of these compounds and multilayer heterostructures of these materials in terms of microstructure and optical and electrical properties. Discussions with other users of ECR plasmas[1] and our own results have led us to be concerned that, as a result of the low bond strength of the surface and near-surface atoms of GaN and InN, there is an increased potential for point defect damage and resulting electrical compensation in these materials. This damage would arise from the interaction of high energy N species with the surface and near-surface regions of these materials during deposition. This is especially true if the plasma power is increased to enhance the flux of the reactive species. Recent research has shown that GaN films grown at higher microwave powers exhibit degraded electrical and luminescent properties as compared to films grown at lower microwave power levels[2-5]. An alternative method of producing atomic nitrogen that minimizes or eliminates the undesirable production of high energy ionic nitrogen is needed. To address this concern, we are currently collaborating with Effusion Science Inc. regarding the design of a novel high-temperature ammonia-cracking source. This report presents the design and testing of the high temperature ammonia cracking source for production of high fluxes of atomic nitrogen as an alternative to the ECR source in GSMBE.

B. Experimental Procedure

The ammonia cracking source manufactured by Effusion Science Inc. has been installed in the sleeve of our currently unused MBE effusion cell (2.25" diameter). Nitride-grade ammonia is used as the source gas and is further purified by a Nanochem ammonia purifier prior to entering the cracker cell. A 0-10 SCCM flow controller is used to adjust the ammonia flux. After entering the cracker cell, the ammonia is decomposed by means of a single bounce delivery off of a wide-area catalytic rhenium filament. Al and Ga fluxes are provided by the normal MBE effusion cells.

A quadrupole mass spectrometer was used to characterize the resulting flux exiting the cracker cell under various filament temperatures and ammonia flow rates. GaN and AlN were then grown using various growth temperatures and III/V flux ratios with and without cracking of the ammonia in the cracker cell. The microstructures of the films were characterized by reflection high energy electron diffraction (RHEED), scanning electron microscopy (SEM) and photoluminescence (PL) analyses.

C. Discussion

The use of cracking ammonia as a source of nitrogen is not new to the field of III-V nitride growth. It is the current method used in growth techniques such as MOCVD and MOVPE where ammonia is cracked on the surface of the substrate, requiring relatively higher growth temperatures to achieve efficient nitrogen production. Several recent successes have been reported in the use of GSMBE utilizing Ga and NH_3 to grow GaN on sapphire substrates [6-9]. Reactive molecular beam epitaxy has also used the cracking of ammonia on the substrate as a nitrogen source[10-11]. Another technique recently used was hot filament enhanced CVD [12,13]. In this process, it is surmised that the catalyzed film growth is initiated through the decomposition of ammonia and subsequent production of NH radicals by a heated tungsten filament. These products trigger further reactions which react with the metalorganic gas to form precursors to film deposition. These precursors then decompose on the heated substrate resulting in film growth[13]. The decomposition of ammonia on various filament surfaces at high temperatures has shown that the two primary reactions that occur are:

$$NH_3 + M \rightarrow NH_2 + H + M \quad (1)$$

$$NH_3 + H \rightarrow NH_2 + H_2 \quad (2)$$

In the case of the catalyzed CVD growth, Reaction 2 is enhanced by the addition of hydrogen to the reaction chamber between the tungsten filament and the heated substrate to aid in the production of NH_2. It is the secondary reactions, primarily the formation of NH radicals, that next occur which are responsible for precursor formation with the metalorganic mentioned above[12-14]. Examples of these secondary reactions include:

$$NH_2 + H \rightarrow NH + H_2 \quad (3)$$

$$NH_2 + NH_2 \rightarrow NH + NH_3 \quad (4)$$

Ammonia Gas Cracker Design. The ammonia cracker was designed to allow the ammonia to decompose primarily to NH_2 while limiting the formation of N_2 by means of a single interaction with a wide-area catalytic Re filament[12,13]. Rhenium was chosen for two reasons: (1) rhenium catalysts are exceptionally resistant to passivation from gases such as nitrogen[15] and (2) hydrogen atoms have been detected in ammonia decomposition reactions on rhenium filaments heated to high temperatures approaching 2000 K[16]. Therefore, it should not be necessary to add hydrogen from some other source to aid in the production of NH_2. Secondary reactions on the substrate surface will produce NH radicals which are highly reactive with the Group III species and result in film growth.

Ammonia Gas Cracker Characterization. The ammonia gas cracker was tested to determine which combination of filament temperature and ammonia flow rate would provide the most efficient source of atomic nitrogen and NH radicals needed for III-V nitride growth. The temperature of the Rhenium filament is measured indirectly by using I-V versus temperature data provided by Effusion Science, Inc. Mass spectrometry was used to measure the resulting mass current intensities resulting from various operating parameters. An example of this data is shown in Fig. 1. Figures 2-4 show the various ratios of mass intensities to that of ammonia.

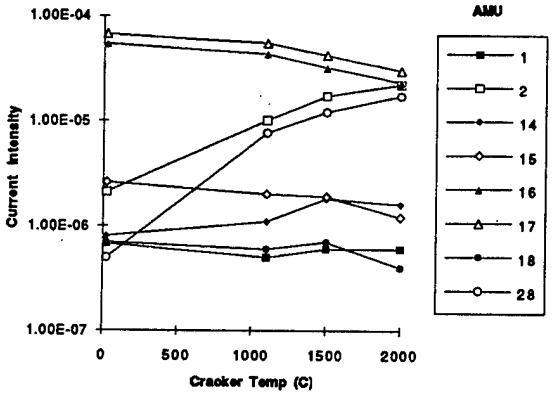

Figure 1. 5.00 SCCM NH_3.

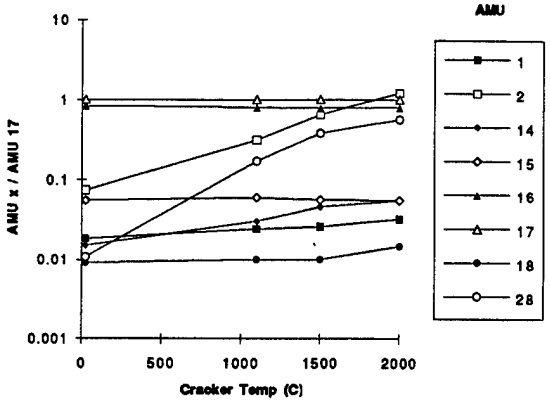

Figure 2. 1.00 SCCM NH_3.

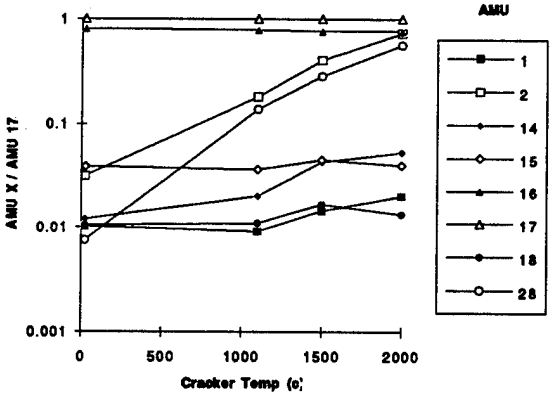

Figure 3. 5.00 SCCM NH_3.

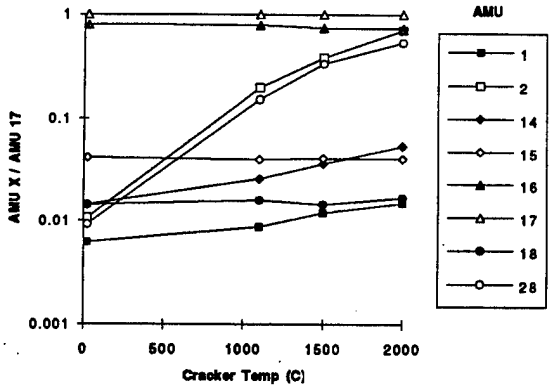

Figure 4. 8.00 SCCM NH_3.

Analysis of the mass spectrometry data revealed that the cracker cell was cracking the ammonia primarily into molecular hydrogen and nitrogen, with very little resulting atomic nitrogen and NH radical species. Since the reactive species are part of the NH_3 cracking pattern in the mass spectrometer itself, providing a detailed discussion on the performance of the cracker cell is difficult. It is surmised that the resulting H_2 and N_2 fluxes are forming from the recombination of NH molecules leaving the surface of the Re filament.

Initial Film Growth. Figures 5-8 show SEM micrographs of GaN deposited directly onto 6H-SiC on-axis wafers provided by Cree Research, Inc. Growth was performed with and without precracking the ammonia in the ammonia cracker. Results reveal that use of the cracker cell to precrack the ammonia leads to a degradation in both film quality and growth rate. By cracking the ammonia directly on the surface of the substrate, a finer and smoother surface morphology is achieved, and the growth rate dramatically increases (in this case 3000A/hr without the cracker versus 1000A/hr with the cracker). These results and the results from the RGA data suggest that the reduced growth rate resulting from use of the cracker cell is a consequence of a reduced ammonia flux reaching the substrate, which in-turn provides a reduced supply of NH radicals necessary for film growth.

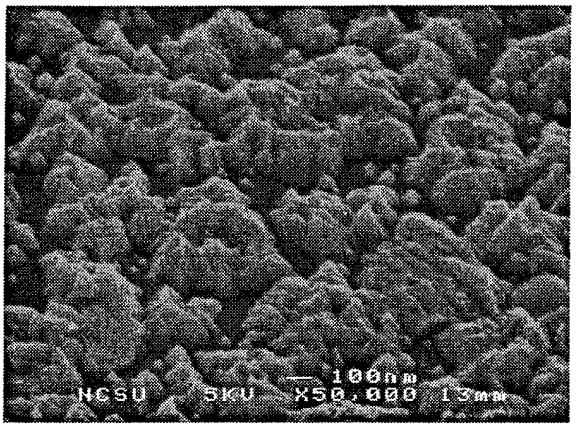

Figure 5. GaN (1000A) on 6H-SiC, precracked NH_3 at 1500C, growth temp 800C.

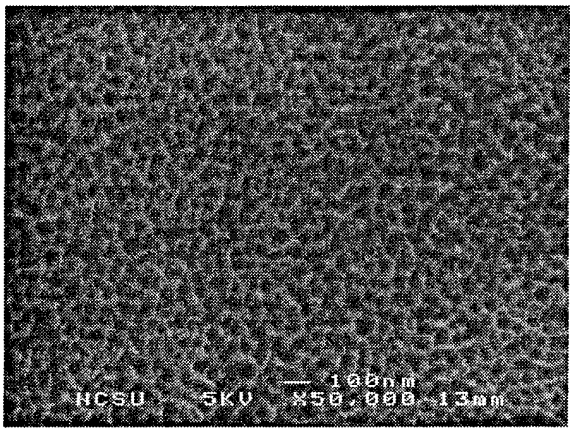

Figure 6. GaN (3000A) on 6H-SiC, no precracking of NH_3, growth temp 800C.

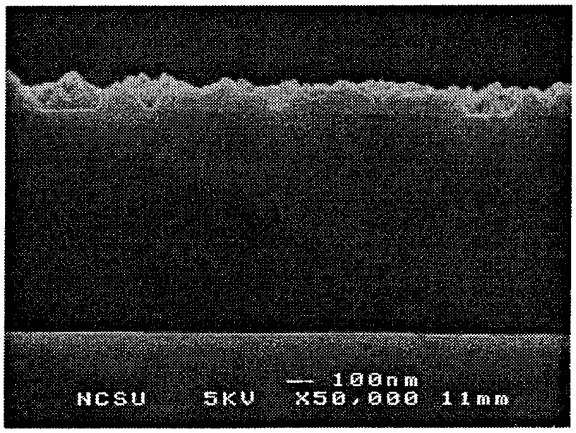

Figure 7. GaN (1000A) on 6H-SiC, precracked NH_3 at 1500C, growth temp 800C.

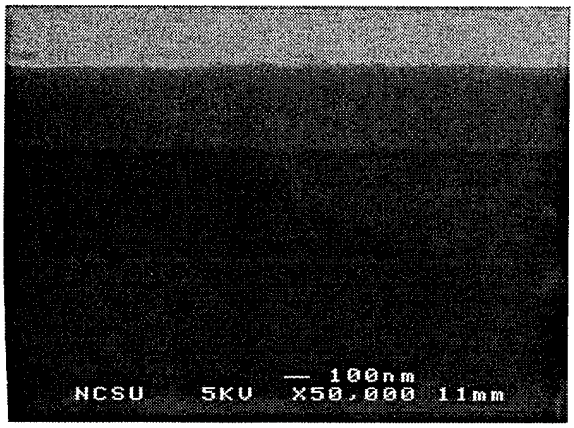

Figure 8. GaN (3000A) on 6H-SiC, no precracking of NH_3, growth temp 800C.

Although the ammonia cracker did not provide us with the necessary flux of atomic nitrogen and NH radicals for enhanced film growth, the use of ammonia as a source for the Group V species has resulted in a significant improvement in the optical properties of the resulting GaN film. Figure 9 shows the PL spectra taken from a sample grown without the assistance of the ammonia cracker cell. This is the first time this laboratory has produced GaN that has resulted in photoluminence at 354 nm, attributed to the recombination of excitons and neutral donors. We have previously used an ECR plasma source for our Group V species, which proved detrimental to the optical quality of the resulting GaN film.

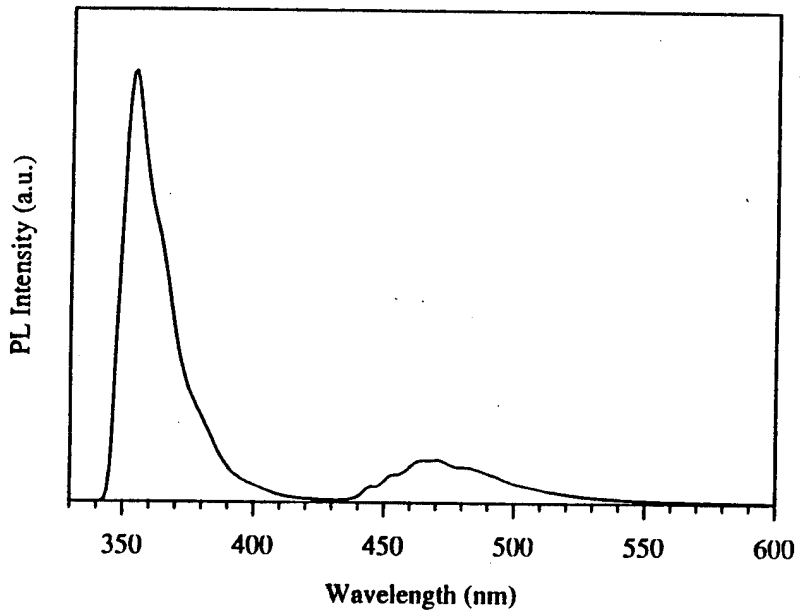

Figure 9. PL of GaN at 8K.

Figures 10-13 show SEM micrographs of AlN grown with and without the assistance of the ammonia cracker. Analysis of these figures reveal that for the case of AlN, no discernible difference occurred in either the morphology or growth rate of the resulting films. Use of NH_3 as the nitrogen source has resulted in our ability to grow AlN at 3000A/hr, whereas growth rates of 1000A/hr were achieved using the ECR plasma source.

D. Conclusions

The use of ammonia (NH_3) thermally cracked on the substrate surface (6H-SiC) has lead to a marked improvement in the optical properties of GSMBE grown GaN as characterized by PL spectrum exhibiting a sharp peak at 354 nm in our films for the first time. By using NH_3 as an alternative source for the ECR, the growth rate of AlN has increased from 1000A to 3000A an hour.

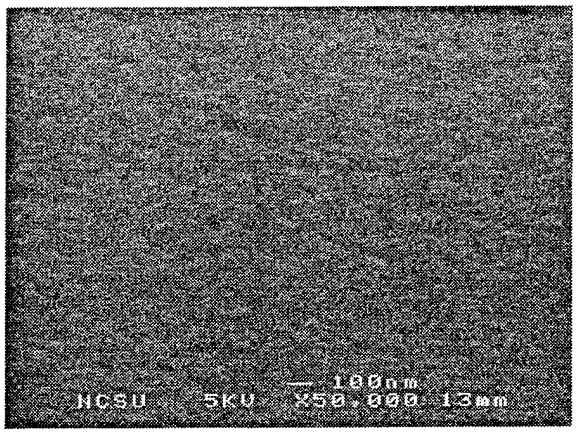

Figure 10. AlN (3000A) on 6H-SiC, precracked at NH_3 1100C, growth temp 1100C.

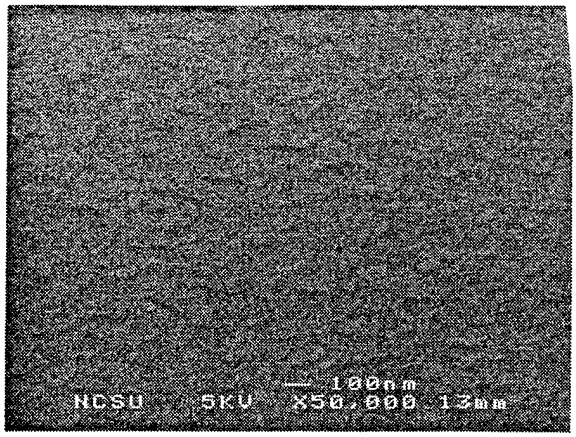

Figure 11. AlN (3000A) on 6H-SiC, no precracking of NH_3, growth temp 1100C.

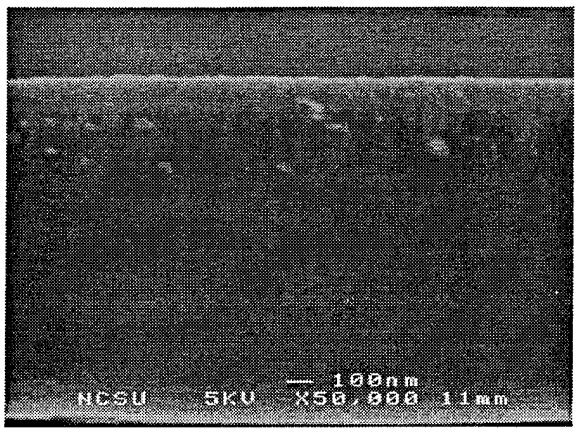

Figure 12. AlN (3000A) on 6H-SiC, precracked at NH_3 1100C, growth temp 1100C

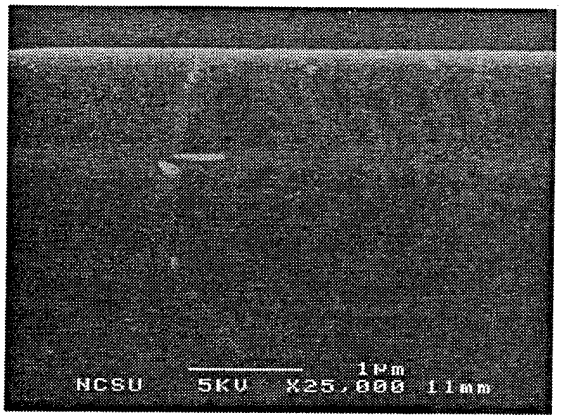

Figure 13. AlN (3000A) on 6H-SiC, no precracking of NH_3, growth temp 1100C

The use of a high-temperature ammonia-cracking source to precrack the ammonia has resulted in the degradation of both the film morphology and growth rate for GaN. The effects of the cracker cell on AlN growth is still inconclusive. Analysis of RGA spectra reveal that molecular nitrogen and hydrogen are the primary constituents resulting from decomposition of the ammonia. Recombination of NH molecules leaving the Re filament surface are thought to be the source of the N_2 and H_2. This subsequently leads to a reduced growth rate for GaN films.

E. Future Research Plans and Goals

Over the next few months, we will attempt to optimize the quality (microstructurally, optically, and electrically) of GaN, AlN and their solid solutions grown by using ammonia as the source of the Group V species. GaN will be grown on both AlN and graded AlGaN buffer layers. We will then investigate methods of doping the films to obtain n- and p-type carriers. Once we have established these abilities, we will employ the technique for development of optical devices. The possibility of using a nitride to replace the Re filament is under consideration at this time. This may allow for an increase in the ratio of atomic N and NH radicals produced by the ammonia cracker which will be required for the efficient growth of InN grown at lower growth temperatures.

F. References

1. S. Strite, IBM Research Report #83986, March 28, 1994 and private discussions.
2. R. J. Molnar, and T. D. Moustakas, J. Appl. Phys. **76,** (8) 4587 (1994).
3. R. C. Powell, N. E. Lee, Y. W. Kim, and J. E. Greene, J. Appl. Phys. **73**, 189 (1993).
4. M. E. Lin, B. Sverdlov, G. L. Zhou, and H. Morkoc, Appl. Phys. Lett. **62**, 3479 (1993).
5. R. Singh, R. J. Molnar, M. S. Unlu, and T. D. Moustakas, Appl. Phys. Lett. **64**, 336 (1994).
6. R. C. Powell, N. E. Lee, and J. E. Greene, Appl. Phys. Lett. **60** (20) 2505 (1992).
7. H. Z. Xiao *et al.*, J. Appl. Phys. **76** (12) 8195 (1994).
8. H. Gotoh, T. Suga, H. Suzuki, and M. Kimata, Jpn. J. Appl. Phys. **20**, L545 (1981).
9. S. Yoshida, S. Misawa, and S. Gonda, Appl. Phys. Lett. **42**, 427 (1983).
10. H. U. Baier and W. Mînch, J. Appl. Phys. **68** (2), 586 (1990).
11 H. U. Baier and W. Mnch, J. Vac. Sci. Technol., B **10** (4) 1735 (1992).
12. J. L. Dupuie and E. Gulari, Appl. Phys. Lett. **59**, 549 (1991).
13. J. L. Dupuie and E. Gulari, J. Vac. Sci. Technol. A **10** (1), 18 (1991).
14. G. S. Selwyn and M. C. Lin, Chemical Physics **67**, 213 (1982).
15. *Handbook of Chemistry and Physics* **73**, 4-24 (1992).
16. S. N. Foner and R. L. Hudson, J. Chem. Phys. **80** (9), 4013 (1984).

IV. Luminescence Studies of GaN, AlN, InN and Their Solid Solutions

A. Introduction

Luminescence is the emission of photons due to excited electrons in the conduction band decaying to their original energy levels in the valance band. The wavelength of the emitted light is directly related to the energy of the transition, by E=hν. Thus, the energy levels of a semiconductor, including radiative transitions between the conduction band, valance band, and exciton, donor, and acceptor levels, can be measured.[1,2] Various methods exist to excite the electrons, including photoluminescence (photon excitation), and cathodoluminesence (electron-beam excitation). In each technique, signal intensity is measured at specific wavelength intervals using a monochromator and a detector. The intensity versus wavelength (or energy) plot can then be used to identify the characteristic energy band gap and exciton levels (intrinsic luminescence) of the semiconductor, and the defect energy levels (extrinsic luminescence) within the gap .[1]

Both photo- and cathodoluminescence analysis has been performed on AlN, GaN, InN and their solid solutions.[3-20] Much of the work has been in the measurement the low temperature luminescence of GaN. High quality, unintentionally doped GaN exhibits a strong donor-bound exciton peak at 357.3 nm (3.47 eV).[16] Defect peaks due to donor-acceptor (DA) transitions and accompanying phonon replicas are also prevalent, with peak wavelengths at 380.3, 391.2 and 402.9 nm. The identity of the acceptor is not clear. A deep emission at 540 nm (2.2 eV) is also common in GaN. Currently the source of this emission is not known, although various models exist to explain it.[19,20] It is of utmost importance to limit the defect transitions, as it can reduce the transition probability of the near-gap emission.

Although undoped GaN is always n-type, recent advances in film growth have lowered the carrier concentration to $10^{16}/cm^3$. For device applications it is important to have a high carrier concentration at a controlled level. Common dopants for n-type doping of GaN include Si and Ge. Nakamura, *et al.* found that for Si-doped GaN, two peaks dominate the spectrum.[12] The first is a UV emission peak at 380 nm. The second peak is the deep level (DL) emission previously discussed; this transition is enhanced by Si-doping. Conflicting results were shown by Murakami, *et al.*, who saw a band edge peak at 358 nm dominate their spectrum.[8] The DL emission at 540 nm in their samples was very weak.

The development of light emitting diodes (LEDs) and laser diodes using GaN-based materials has been limited by the difficulty in obtaining quality p-type films.[12] Common dopants include Zn, Cd, and Mg.[3] Recent work has proven successful, with low resistivity Mg-doped GaN obtained by thermal annealing or low energy electron beam irradiation

(LEEBI) as a post-growth process step. The luminescence from these films typically show a broad peak located at 450 nm, with no emission near the band-edge.

Work on AlN and $Al_xGa_{1-x}N$ has been limited by the energy gap of 6.2 eV for AlN. This corresponds to a wavelength (200 nm) that is lower than most of the optical light sources. An excimer laser using the ArF line (193 nm) could possibly be used, although very little work on this has been done to date.[30] Cathodoluminescence of AlN and $Al_xGa_{1-x}N$ is possible, however, and most of the results have been obtained via this method.[16-18,30-33] $Al_xGa_{1-x}N$ with low amounts of Al can also be investigated using frequency doubled and tripled lasers that have lines down to 244 nm.

B. Experimental Procedures

A combined photo- and cathodoluminesence system is used to measure the luminescence from the III-V nitrides. A schematic view is shown in Fig. 1, and a block diagram is shown in Fig. 2. Each sample is attached to a cryostat that allows for a test temperature range of 6 to 300 K. A McPherson model 219 vacuum monochromator with a focusing mirror chamber is used to collect the emitted light. The focal length of the monochromator is .5 m, with a wavelength resolution of .04 nm at 313.1 nm for a 1200 G/mm grating. A photon counting detection scheme is used to measure the light intensity, with a Photomultiplier tube (PMT) used that has a wavelength range of 180-650 nm.

A Liconix He-Cd laser is the photoexcitation source. It is a continuous wavelength laser that operates at a wavelength of 325 nm (3.8 eV), with a power of 15 mW. It is used for PL of GaN and $In_xGa_{1-x}N$, but a lower wavelength source is needed to test the full range of $Al_xGa_{1-x}N$ solid solutions.

A Kimball Physics electron gun is used for cathodoluminesence measurements. It has maximum beam voltage of 10 keV and a maximum beam current of 450 uA. By varying the beam voltage it is possible to perform depth-resolved spectroscopy. The beam blanking capability of the electron gun will allow for time-delay studies of the semiconductors.

C. Results and Discussion

Undoped GaN. Photoluminescence measurements were performed on GaN films grown via OMVPE on vicinal α(6H)-SiC(0001)$_{Si}$ wafers. The buffer layer for each sample was AlN. All of the tests were performed at 8 K, unless otherwise noted.

The photoluminescence of undoped GaN grown at 950 °C is shown in Fig. 3. The sample thickness was 1 μm. The peak at 357.36 nm was attributed to the recombination of excitons at neutral donors.[27] The FWHM of this peak, 4 meV, indicates the high quality of the sample. A weak defect peak ascribed to donor-acceptor (DA) pair recombination was observed at 379 nm (3.26 eV) with two associated LO-phonon replicas only after a 250X magnification of

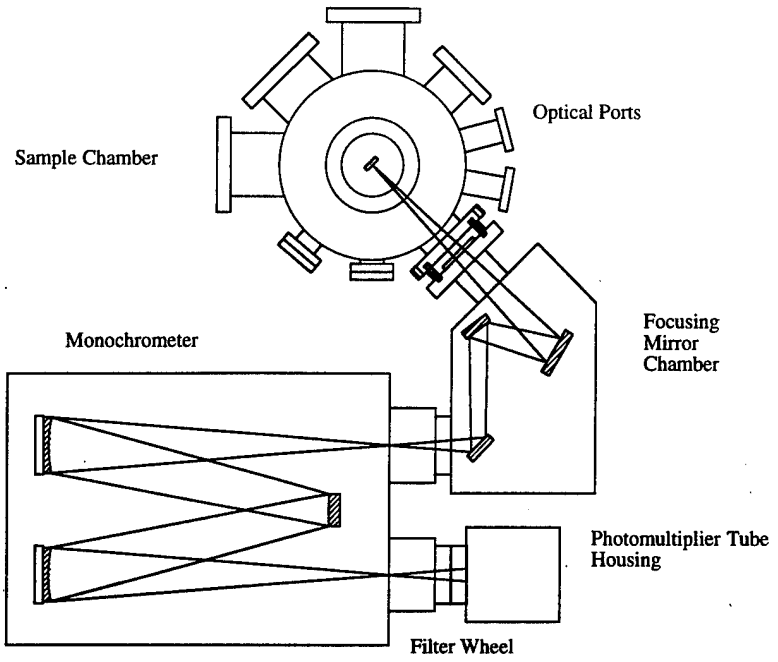

Figure 1. Schematic view of combined photo- and cathodoluminescence system.

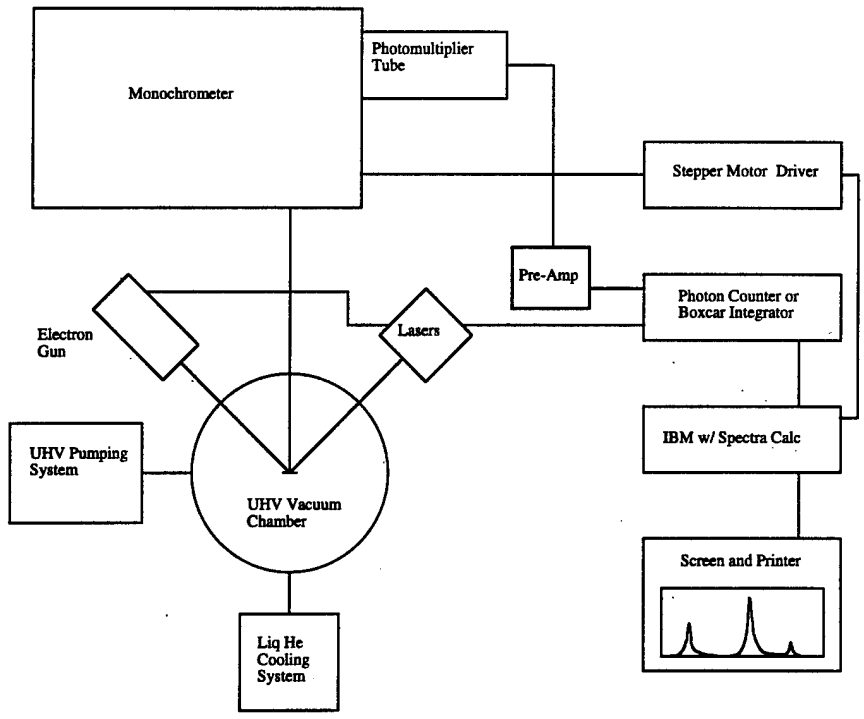

Figure 2. Block diagram of combined photo- and cathodoluminescence system.

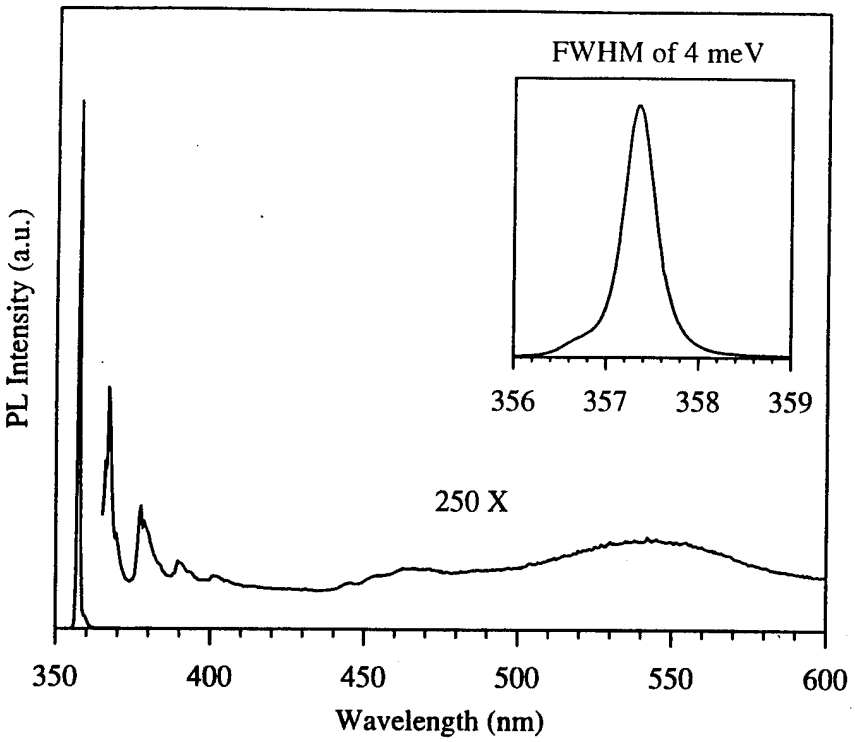

Figure 3. PL of GaN on SiC(0001) at 8 K.

the spectrum.[25] The origin of the D-A pair is attributed to residual donors and acceptors. Two LO-phonon replicas of the bound-exciton peak and a broad peak centered at 545 nm (≈2.2 eV), commonly associated with deep-levels (DL) in the bandgap, were also observed at this magnification.[26]

Photoluminescence of GaN at various film thicknesses revealed a shift in the donor-bound exciton peak to lower energy as film thickness increased. The results are shown in Fig. 4, and the thickness and peak position for each film is given in Table I. The shift may be attributed to a change in the bandgap due to tensile strain in the film.[29] This is ascribed to the thermal expansion mismatch between GaN and the SiC substrate, which upon cooling of the film after growth results in the films being under tension. From this data it appears that as thickness increases the tension in the film also increases. Further studies will be done in the future to verify this.

Mg-doped GaN. The doping of GaN with magnesium to obtain p-type electrical behavior proved to be successful. The PL of Mg-doped GaN at 8 K as a function of annealing conditions is shown in Fig. 5. The growth temperature was 1050 °C, and the Cp_2Mg flow rate was .5 μmoles/min. The sample as-grown was p-type, but electrical measurement could not be made because the structural quality of the material was poor (possibly due to the high concentration of Mg).

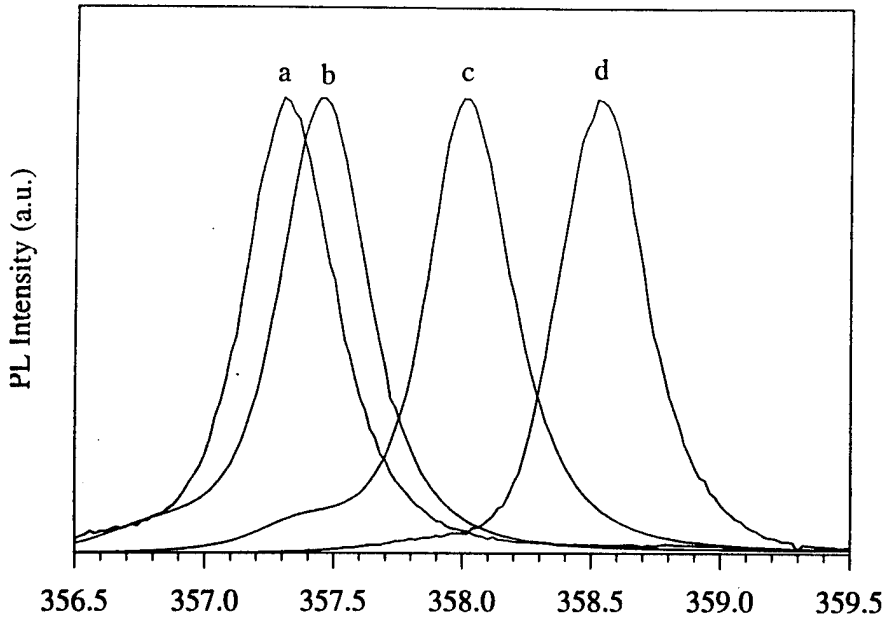

Figure 4. PL of GaN on SiC(0001) at 8 K for various thicknesses.

Table I

Sample	Film Thickness (μm)	Peak Location (nm)
a	.7	357.30
b	.9	357.46
c	1.4	358.00
d	2.7	358.52

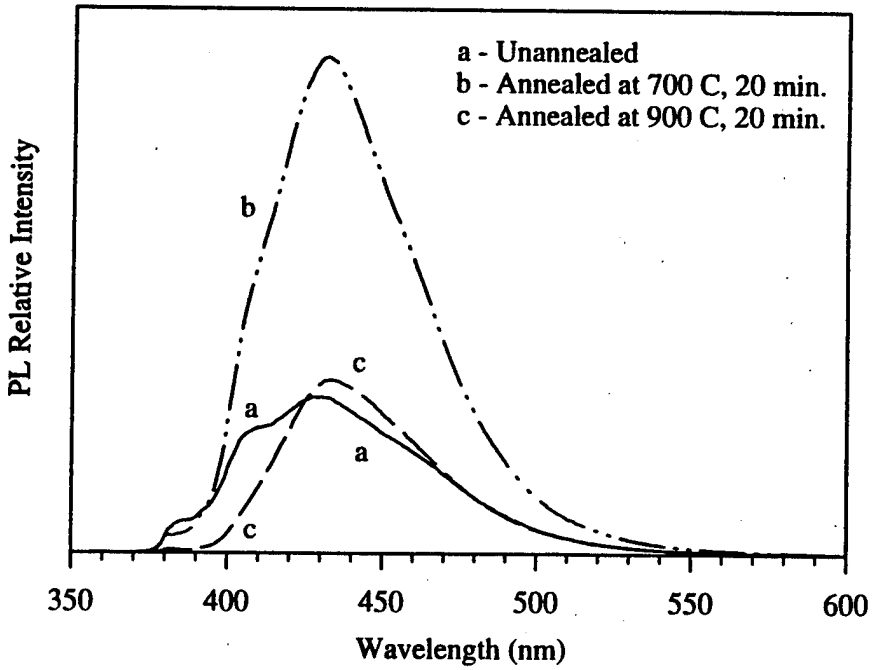

Figure 5. PL at 8 K of p-type Mg-doped GaN.

Annealing at 700 °C for 20 minutes enhanced the luminescence intensity by 250 %. Post-growth annealing is thought to release Mg from Mg-H complexes, which passivate the acceptors [22]. Recent work has shown that Mg-H complexes form at 500-600 °C for MBE-grown samples annealed in H_2 [24].

Annealing at 900 °C for 20 minutes resulted in a sharp decrease in the PL intensity compared to the sample annealed at 700 °C. This result is in line with previous work, which showed that PL intensity decreased gradually as the annealing was increased past 500 °C, while the resistivity of the sample did not change [22]. Thus the decrease in PL intensity is not due to a change in the number of active acceptor levels through compensation or other mechanisms.

One possibility is the thermal expansion mismatch between the GaN and the SiC substrate. As the annealing temperature is increased the temperature range over which the sample is later cooled is also increased. This leads to an increase in the stresses generated by the mismatch in thermal expansion. The resulting elastic strain is thought to lower the overall PL efficiency of the sample by increasing the rate of non-radiative transitions.

The effect of growth temperature for Mg-doped GaN was also investigated. The Cp_2Mg flow was .2 μmoles/min at each temperature, which was lower than the sample discussed previously. Previous work has shown that Mg concentration in GaN at a given flow rate is almost independent of substrate temperature for a range of 850-1100 °C [23].

The PL spectrum of the sample grown at 975 °C is shown in Fig. 6. The unannealed sample exhibited relatively weak donor-acceptor (D-A) pair emission, along with its LO-phonon replicas, and a broad peak at 481 nm. The origin of the D-A pair was attributed to residual donors and the doped Mg-acceptors. The origin of the 481 nm peak was unknown, but it has been seen in other samples that were grown at lower temperatures. After annealing at 900 °C for 20 minutes the PL emission was very weak. This indicates that a sample growth temperature of 975 °C is too low.

The PL spectrum of the sample grown at 1050 °C is shown in Fig. 7. For the unannealed sample the D-A peak and its LO-phonon replicas were the dominate feature in the spectrum, and the peak intensity was 320 times stronger than the sample grown at 975°C. There was no evidence of the peak at 481 nm, although it could have been overwhelmed by the intensity of the D-A peaks.

Annealing of the sample at 900 °C for 20 minutes results in a shift of the PL spectrum to lower energy, with the peak emission at 406 nm. The peak intensity of this sample is .6 % of the unannealed sample. Annealing of the sample for an additional 20 minutes further decreased the PL intensity.

The PL spectrum for the sample grown at 1100 °C before annealing is shown in Fig. 8. The peak emission is at 429 nm. This sample was p-type as-grown, with a room-temperature hole concentration of $2\times10^{16}/cm^3$.

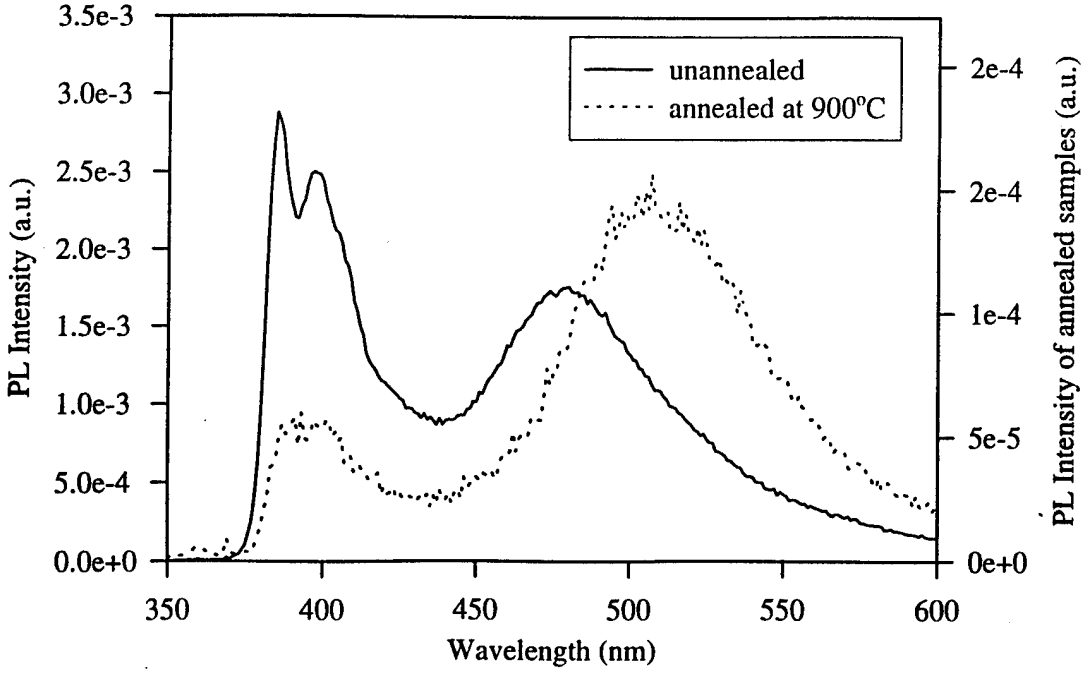

Figure 6. PL at 8 K of p-type Mg-doped GaN grown at 950°C.

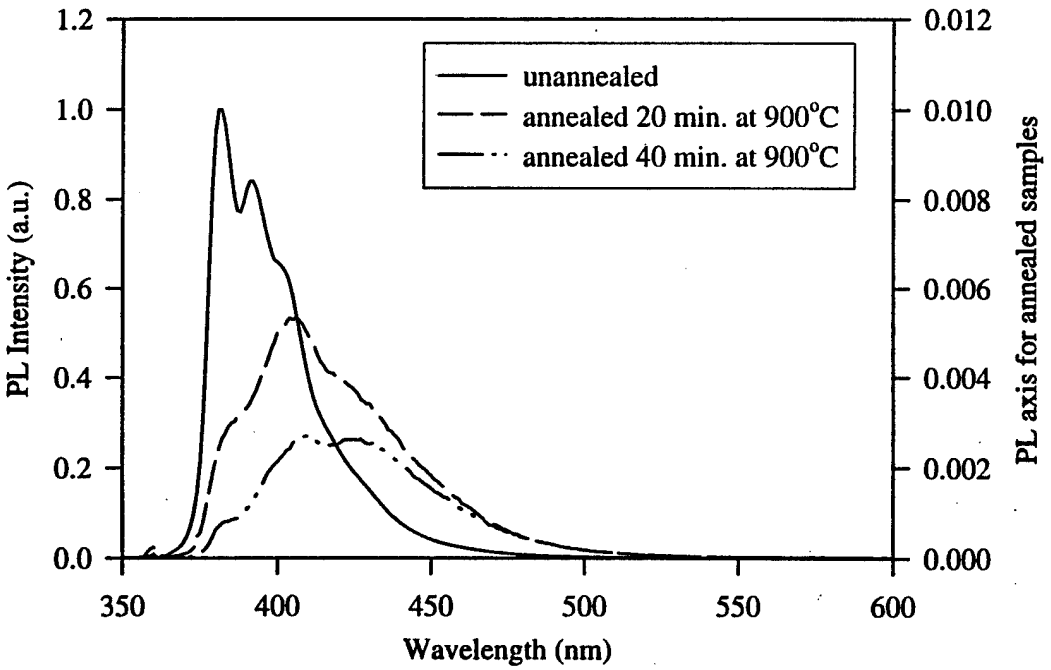

Figure 7. PL at 8 K of p-type Mg-doped GaN grown at 1050°C.

The PL spectrum at room temperature of the Mg-doped GaN as-grown and annealed at 600 and 700 °C is shown in Figure 9. The peak emission was at 460 nm for the as-grown sample and at 456 nm for the two annealed samples. The PL intensity was highest for the sample annealed at 600 °C and decreased at 700 °C, confirming that the PL intensity decreases for

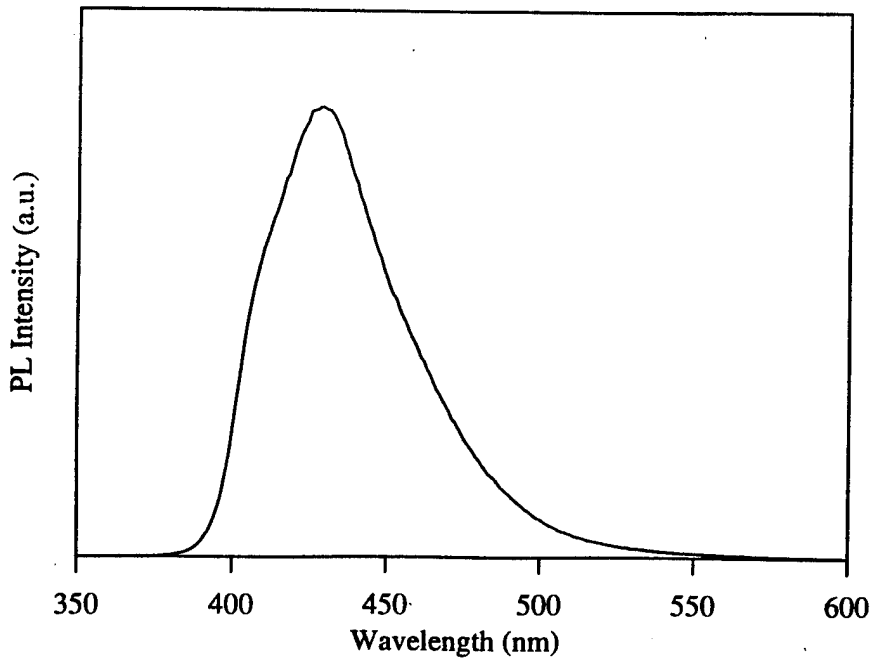

Figure 8. PL at 8 K of p-type Mg-doped GaN unannealed, grown at 1100°C.

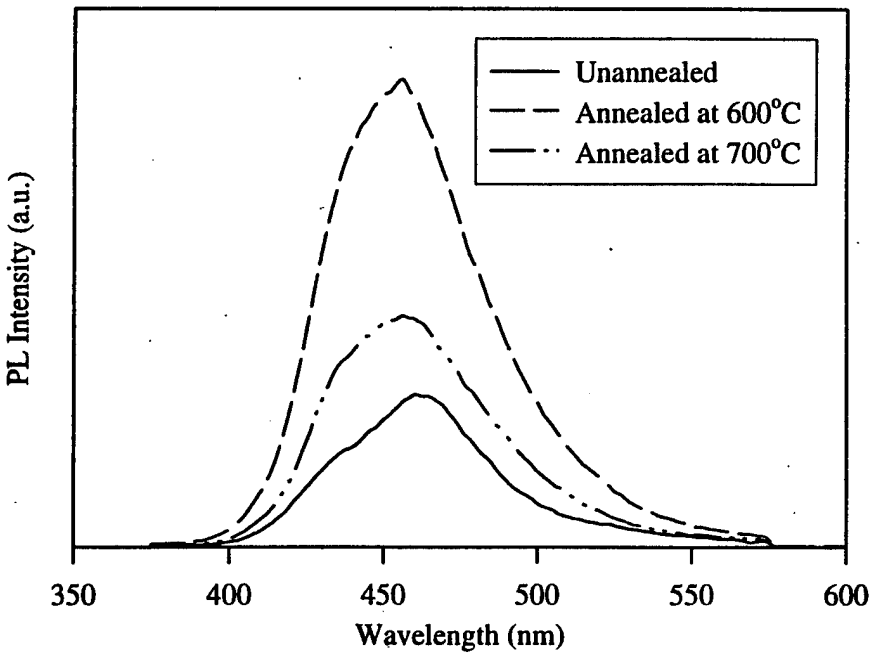

Figure 9. PL at room temperature of p-type Mg-doped GaN grown at 1100°C.

higher annealing temperatures. The room temperature hole concentration was $1\times10^{18}/cm^3$ for the sample annealed at 600 °C. This value did not change for higher annealing temperatures, as seen in previous work.

CL of AlGaN. Cathodoluminescence was performed on $Al_xGa_{1-x}N$ samples grown directly on vicinal α(6H)-SiC(0001)$_{Si}$ wafers. Each test was performed at 8K with a beam voltage of 7 keV and a beam current of 200 μA. Four samples were tested, and the results are shown in Fig. 10. The band-edge peak location, the peak FWHM, and the thickness of each sample is presented in Table II. The composition of each sample is not known, but it will be measured using SIMS in the future.

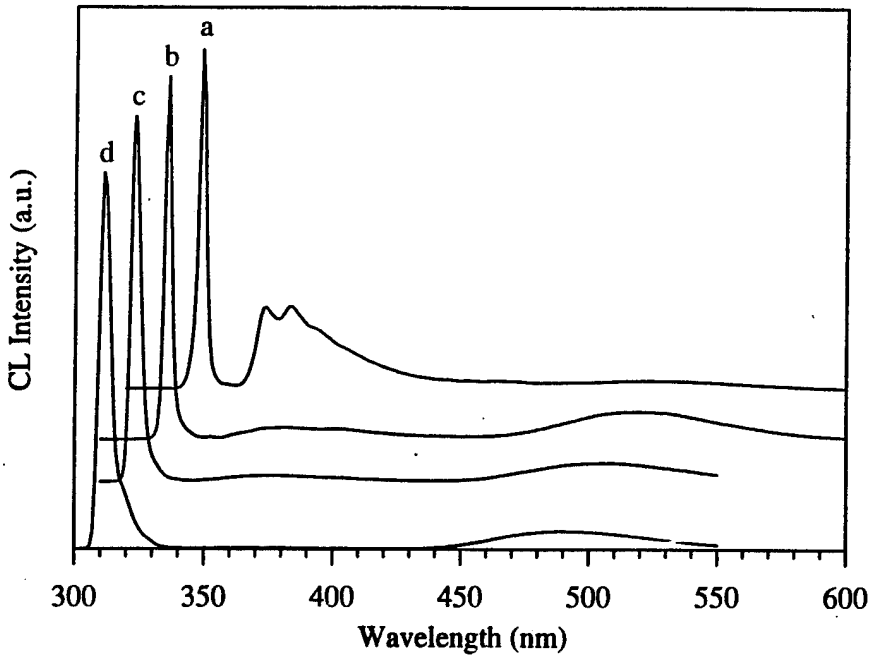

Figure 10. CL of $Al_xGa_{1-x}N$ at 8 K.

Table II

Sample	Peak Location (nm)	FWHM (meV)
a	349.3	31
b	334.6	46
c	324.5	59
d	311.4	64

As expected, the FWHM of the band-edge peak increases as x increases due to alloy broadening.[28] Given this, along with the absence of a buffer layer, the CL for these samples is still quite strong. Samples grown on on-axis SiC exhibited weaker band-edge CL emission.

Figure 11 shows the spectrum below the band-edge enhanced. Sample *a* exhibits relatively strong emission at 374 nm with two phonon replicas that are attributed to D-A pair emission.

As x increases the peaks attributed to D-A pair emission move to higher energies, but they are not as easily resolved. This could also be attributed to alloy broadening.

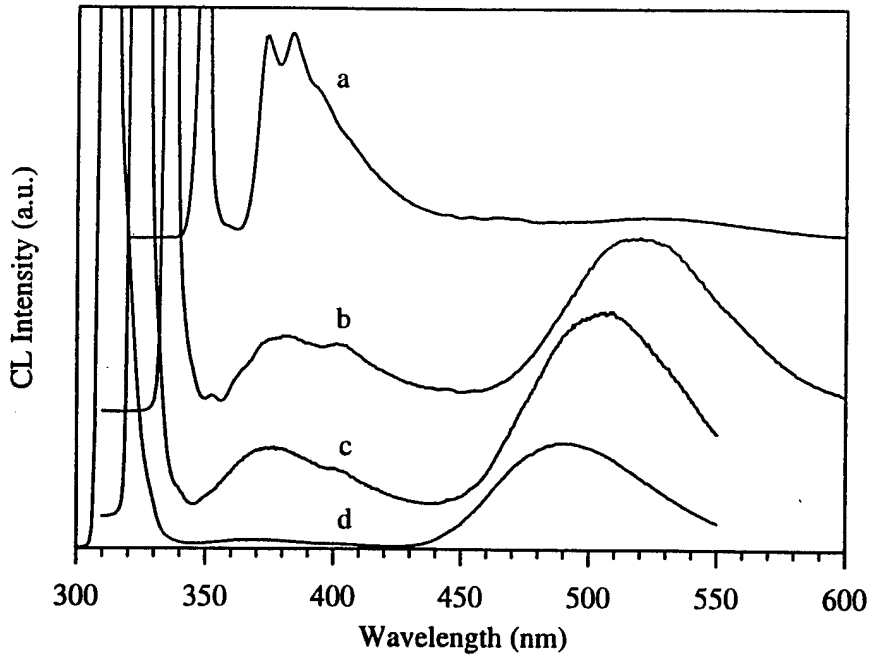

Figure 11. CL of $Al_xGa_{1-x}N$ at 8 K.

As x increases the DL emission centered at 540 nm for GaN also moves to higher energy. Previous work has studied the PL of GaN as a function of pressure to model the $Al_xGa_{1-x}N$ system.[34] Results showed that for pressures up to 20 GPa the pressure coefficient of the DL luminescence is equal to the pressure coefficient of the band gap. Using the pressure coefficient of 30 meV/GPa for the band gap they found that the change in the energy of the DL emission is equal to the change in the energy of the band-gap up to .6 eV. After 20 GPa they propose that a resonant state in the conduction band crosses over into the gap, and then the DL luminescence should be due a transition from the resonance-derived deep state to the same deep acceptor state. This resonant state is due to the nitrogen vacancy, which they suggest is the native donor in GaN.

This model for $Al_xGa_{1-x}N$ was tested using the CL data for samples *a-d*, along with other alloy samples grown on both vicinal and on-axis α(6H)-$SiC(0001)_{Si}$ wafers. PL of AlGaN tested at OSU are also included (discussed in next section). The results are shown in Fig. 12. The change in energy of the DL emission (E_{DL}) follows the change in energy of the band-edge emission (E_{BE}) initially, but after .2 eV it begins to lag behind. Thus it does appear that the luminescence of AlGaN follows the behavior seen in the pressure experiments of GaN, although further testing will be done to confirm this.

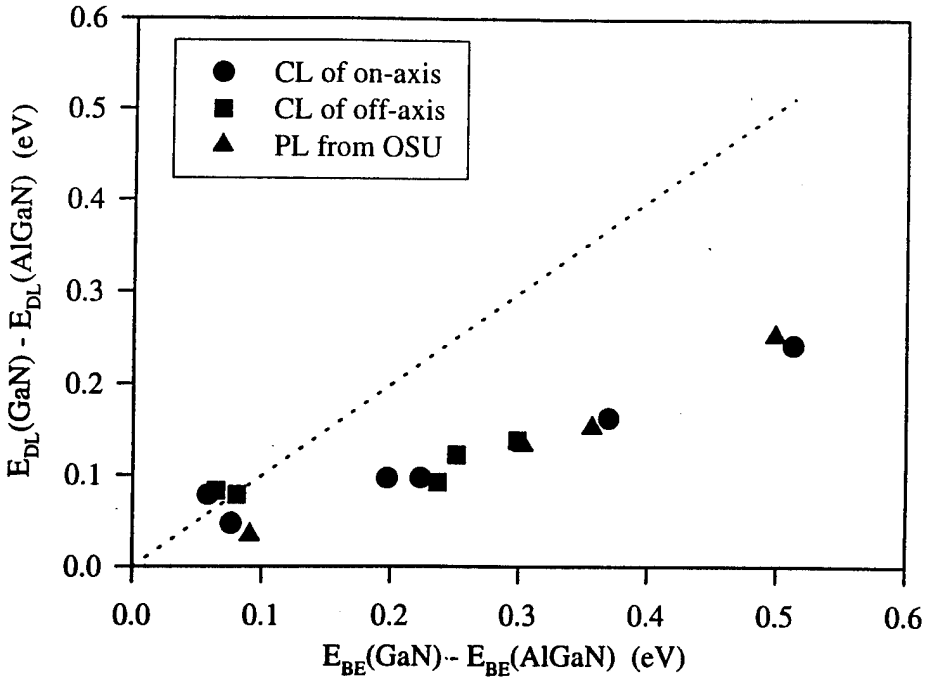

Figure 12. Change in deep level peak emission vs. change in band-edge emission.

PL of AlGaN (In Collaboration with Oklahoma State University). Photoluminescence of $Al_xGa_{1-x}N$ through a collaboration with the Center for Laser Research at Oklahoma State University was performed. The excitation source is a frequency-doubled 488 nm line of an Ar-ion laser, which results in an output wavelength of 244 nm. Each test was performed at 10 K. PL of two samples is shown in Figure 13, these are samples *c* and *d* from the previous section.

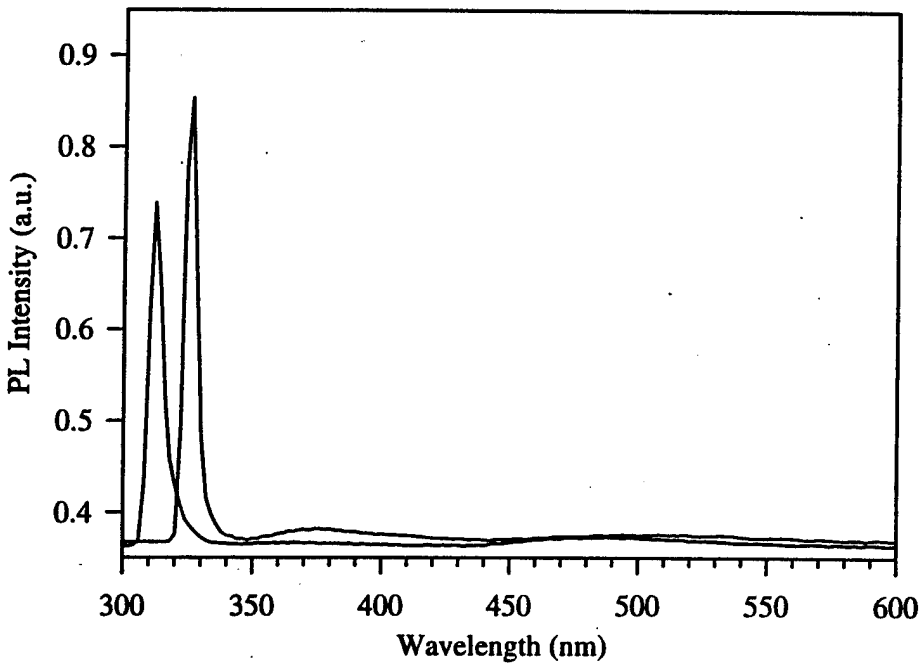

Figure 13. Photoluminescence of $Al_xGa_{1-x}N$ at 10 K using a frequency-doubled 488 nm.

The results indicate that photoluminescence and cathodoluminescence of $Al_xGa_{1-x}N$ give complimentary results. In the future, time-resolved PL will be performed on these and other samples using the frequency-doubled laser.

D. Conclusions

Low temperature (8K) photoluminescence has been used to characterize both undoped and doped GaN films deposited on vicinal $\alpha(6H)\text{-}SiC(0001)_{Si}$ wafers by OMVPE. Unintentionally doped GaN exhibited a sharp peak at 357.36 nm for a 1 μm film that is due to the recombination of excitons at neutral donors. The peak FWHM of 4 meV is an indication of the high quality of the film. The donor-acceptor pair emission and deep level emission at 2.2 eV were very weak for this sample, a further indication of its high quality.

A shift in the donor bound exciton peak to lower energies was found as film thickness increased. This may be due to an increase in residual tensile strain due to the thermal expansion mismatch between GaN and the SiC substrate.

Magnesium doping of GaN proved to be successful. Annealing of GaN at 700°C improved the PL emission by 250 %, but annealing at higher temperatures decreased the PL intensity. Residual strain due to the cooling of the sample after annealing may lead to an increase in non-radiative transitions.

The optimal growth temperature of Mg-doping of GaN was found to be 1100°C. This sample proved to be p-type as grown, with a room-temperature hole concentration of $2\times10^{16}/cm^3$. The PL emission peak was located at 429 nm at 8K and 460 nm at room temperature. Annealing at 600°C improved the room temperature hole concentration to $1\times10^{18}/cm^3$, this value did not improve with annealing at higher temperatures. From this information and the room temperature PL data it is concluded that 600°C is the optimal annealing temperature.

Cathodoluminescence at 8 K was used to characterize $Al_xGa_{1-x}N$ grown directly on vicinal $\alpha(6H)\text{-}SiC(0001)_{Si}$ wafers. The results showed strong emission at the band edge relative to deep level emission. The FWHM of the band edge peak increased with x, as expected.

The shift in the deep level (DL) emission relative to the shift in the band edge emission was investigated and compared to recent work on the pressure dependence of the PL of GaN. The results show that the shift in the DL emission does not keep up with the shift in the band edge emission past .1 eV. Further work will be performed to verify and understand this.

Photoluminescence of $Al_xGa_{1-x}N$ was performed in collaboration with the Center for Laser Research at Oklahoma State University. The results were very similar to CL performed on the same samples. Future work will center on using the PL system to perform time-resolved spectroscopy of $Al_xGa_{1-x}N$.

E. Future Research Plans and Goals

Photoluminescence and cathodoluminescence will continue to be used to measure the quality of GaN films grown by OMVPE and MBE. Work on both p- and n-type doped GaN will also continue. In addition, PL will be used to guide the growth of $In_xGa_{1-x}N$.

Extensive work will be done to study the $Al_xGa_{1-x}N$ alloy system. CL measurements of $Al_xGa_{1-x}N$ films through the full composition range will be performed, and the bowing parameter will be calculated. SIMS and Auger spectroscopy will be performed on the films to measure their exact composition to assist in this work. Ellipsometry and X-ray diffraction will also be used to study these films.

Future collaboration include working with Dr. J.J. Song and Dr. Wei Shan at Oklahoma State on photopumping and time-resolved spectroscopy of $Al_xGa_{1-x}N$ and $In_xGa_{1-x}N$. Deep level transient spectroscopy (DLTS) measurements on $Al_xGa_{1-x}N$ will be made with the assistance of Dr. Nobel Johnson at Xerox PARC. Photoluminescence excitation (PLE) spectroscopy and Optically detected magnetic resonance (ODMR) will be used to study the nature of the deep level emissions in $Al_xGa_{1-x}N$. This work will be done with Dr. Jaime Freitas and Dr. Evan Glaser at the Naval Research Laboratory.

F. References

1. B. G. Yacobi and D. B. Holt, *Cathodoluminescence Microscopy of Inorganic Solids*, Plenum Press, New York (1990).
2. Micheal D. Lumb, Ed., *Luminescence Spectroscopy*, Academic Press, New York (1978).
3. S. Strite and H. Morkoç, J. Vac. Sci. Technol. B **10** (4), 1237 (1992).
4. R. A. Youngman and J. H. Harris, J. Am. Ceram. Soc. **73** [11], 3238 (1990).
5. S. Nakamura, T. Mukai, and M. Senoh, Jpn. J. Appl. Phys. **30** (10A), 1708 (1991).
6. V. F. Veselov, A. V. Dobrynin, G. A. Naida, P. A. Pundur, E. A. Slotensietse, and E. B. Sokolov, Inorganic Materials **25** (9), 1250 (1989).
7. J. N. Kuznia, M. A. Kahn, D. T. Olson, R. Haplan, and J. Freitas, J. Appl. Phys. **73** (9), 4700 (1993).
8. H. Murakami, T. Asahi, H. Amano, K. Hiramatsu, N. Sawaki, and I. Akasaki, J.Crystal Growth **115**, 648 (1991).
9. K. Maier, J. Schneider, I. Akasaki, and H. Amano, Jpn. J. Appl. Phys., **32** (6), 846 (1993).
10. I. Akasaki, and H. Amano, J. Crystal Growth, **99**, 375 (1990).
11. S. Yoshida, H. Okumura, S. Misawa, and E. Sakuma, Surf. Sci. **267** (7), 50 (1992).
12. S. Nakamura, T. Mukai, and M. Senoh, Jpn. J. Appl. Phys., **31** (9), 2883 (1992).
13. S. Nakamura, N. Iwasa, T. Mukai, and M. Senoh, Jpn. J. Appl. Phys., **31** (5), 107 (1992).
14. S. Nakamura, T. Mukai, and M. Senoh, Jpn. J. Appl. Phys., **30** (12A), 1998 (1991).
15. S. Strite, J. Ruan, Z. Li, N Manning, A. Salvador, H. Chen, D. J. Smith, W. J. Choyke, and H. Morkoç, J. Va. Sci. Technol. B **9** (4), 1924 (1991).
16. W. J. Choyke and I. Linkov, Inst. Phys. Conf. Ser. **137**, 141 (1993).
17. S. Pacesova and L. Jastrabik, 1979 Phys. Stat. Sol. B **93**, K111.
18. S. Yoshida, S. Misowa, Y. Fujii, S. Takada, H. Hayakawa, S. Gonda, A. and Itoh, J. Vac. Sci. Technol. **16** (4), 990-3 (1979).

19. E. R. Glaser, T. A. Kennedy, H. C. Crookham, J. A. Freitas, Jr., M. Asif Khan, D. T. Olson, and J. N. Kuznia, Appl. Phys. Lett. **63** (19), 2673 (1993).
20. E. R. Glaser, T. A. Kennedy, J. A. Freitas, Jr., M. Asif Khan, D. T. Olson, and J. N. Kuznia, from the Fifth International Conference on Silicon Carbide and Related Materials in Washington, D.C., Nov. 1993, to be published in the "International Institute of Physics Conferences" Series.
21. T. Sasaki, T. Matsuoka, A. Katsui, Appl. Surf. Sci. **41/42**, 504 (1989).
22. S. Nakamura, N. Iwasa, T. Mukai, and M. Senoh, Jpn. J. Appl. Phys. **31** (5A), 1258 (1992).
23. I. Akasaki, and H. Amano, J. Electrochem. Soc. **141** (8), 2266 (1994).
24. M. S. Brandt, N. M. Johnson, R. J. Molnar, R. Singh, and T. D. Moustakas, Appl. Phys. Lett. **64** (17), 2264 (1994).
25. R. Dingle and M. Ilegems, Solid State Commun. **9**, 175 (1971).
26. W. Götz, N. M. Johnson, R. A. Street, H. Amano, and I. Akasaki, Appl. Phys. Lett., **66**, 1340 (1995).
27. R. Dingle, D. D. Sell, S. E. Stokowski, and M. Ilegems, Phys. Rev. B. **4**, 1211 (1971).
28. E. F. Schubert, E.O. Gobel, Y. Horikoshi, K. Ploog, and H.J. Queisser, Phys. Rev. B. **30** (2), 813 (1984).
29. J. I. Pankove, *Optical Processes in Semiconductors*, Dover Publications, New York (1971).
30. M. A. Khan, D. T. Olson, and J. N. Juznia, Appl. Phys. Lett. **65** (1), 64 (1994).
31. K. Itoh, H. Amano, K. Hiramatsu and I. Akasaki, Jpn. J. Appl. Phys. **30** (8), 1604 (1991).
32. M. A. Khan, R. A. Skogman, R. G. Schulze, and M. Gershenzon, Appl. Phys. Lett. **43** (5), 492 (1983).
33. J. Hagen, R. D. Metcalf, D. Wickenden, and W. Clark, J. Phys. C **11**, 1143 (1978).
34. P. Perlin, T. Suski, H. Teisseyre, M. Leszczynski, I. Grzegory, J. Jun, S. Porowski, P. Boguslawski, J. Bernholc, J. C. Chervin, A. Polian, and T. D. Moustakas, to be published.

V. Reactive Ion Etching of GaN, AlN and InN

A. Introduction

Semiconductor devices are the principle components of electronic and telecommunications systems[1]. In order to densely pack these microscopic components, unidirectional, or anisotropic, etching techniques are required to produce a fine network of uniformly thick lines. Wet etching processes found in many semiconductor manufacturing steps produce multi-directional, or isotropically, etched features with variable thickness through its depth. This is undesirable for microcircuitry since the goal is to produce the smallest devices possible. Therefore, plasma-assisted processes, such as reactive ion etching (RIE), combine the physical characteristics of sputtering with the chemical activity of reactive species to produce a highly directional feature. RIE has the added advantage of providing a more uniform etch and a higher degree of material etch selectivity.

RIE has been employed to etch a wide variety of semiconductor materials including silicon-based materials[2-11], metals, like aluminum[7, 12-18] and III-V compounds, such as GaAs and InP[19-21]. Plasma-assisted etching of newer III-V compounds, such as GaN, AlN and InN, has also been investigated in depth by Pearton *et al.*[22-27] and other investigators[20, 21, 28-31]. There has been widespread interest in using these nitrides for semiconductor device applications requiring visible light emission, high temperature operation and high electron velocities. Since these materials possess wide bandgaps and optical emissions spectra in the blue to near ultraviolet range, they are prime candidates for ultraviolet detection devices.

The objectives of this report are to discuss recent progress made in the field of reactive ion etching of gallium, aluminum and indium nitride. In the following sections, a brief review of pertinent literature on plasma-assisted etching of III-V nitride compounds is provided along with a description of the reactive ion etching system, choice of process gases and results to date.

B. Literature Review

Etching of GaN. Since GaN is a direct transition material with a bandgap ranging from 3.4-6.2 eV at room temperature, it is an ideal candidate for the fabrication of shortwave length light emitters[20, 32]. High quality GaN films have been successfully grown by MOVPE[32], ECR-MBE[33, 34], MOCVD[35] and a layer-by-layer process[36] on a number of substrates. In order to fabricate complete device structures, reliable etching processes need to be developed. Though wet etchants for GaN have been employed, including $NaOH/H_2O$[23, 37] and hot H_3PO_4[37-40], patterning for device fabrication with wet etchants has not been studied or characterized. Thus, RIE is an effective method for the production of fine line patterning in GaN and does not involve direct exposure to heated, concentrated acid and base solutions.

There have been many reports of etching GaN by plasma-assisted processes in the past two years[20-23, 25, 27-31]. The more conventional technique of plasma etching of III-V nitrides, i.e. reactive ion etching, has been employed by several research groups[21-23, 25, 28, 31]. Fairly high etch rates have been attained with chlorine-based plasmas, as shown in Table I. In the chlorine-based plasmas, the higher etch rates are the result of more active Cl species diffusing to the nitride surface. Thus, as the pressure increases more Cl species are available for reaction and the etch rates increase (as shown in the case for BCl_3/Ar plasma). The addition of H_2 to a Cl_2 plasma is believed to tie up nitrogen atoms on the surface as volatile NH_x, resulting in increased etch rates with increasing H_2 flow rates[23]. In addition, there is evidence from Auger electron spectroscopy (AES)[25, 28, 31] that GaN remains stoichiometric after etching and that Cl species are completely reacted and removed from the nitride surface. The AES results concurrently showed that the concentration of oxygen had increased after etching, probably the result of oxygen diffusion to the damaged surface. The source of oxygen was not elucidated, however, water vapor present in the vacuum system may account for a reaction with the GaN surface. Lastly, Adesida *et al.*[28] have demonstrated that fluorine plasmas are impractical to use as etchant gases due to the formation of involitile fluorides with

Table I. Etch Rate Parameters for RIE of GaN

Maximum Etch Rate (Å/min)	Plasma Gases	Pressure (mtorr)	Power* (watts)	DC Bias (-V)	Ref.
175	BCl_3/Ar	1	200 (MW)	250	[23]
510	BCl_3/Ar	50	200 (RF)	NM#	[31]
750	Cl_2/H_2	1	1000 (MW)	150	[25]
200	Cl_2/H_2	1	200 (MW)	150	[25]
200	CCl_2F_2/Ar	1	200 (MW)	250	[23]
139	CCl_2F_2/Ar	20	40 (RF)	NM	[21]
80	CH_4/H_2/Ar	1	200 (MW)	300	[23]
350	CH_4/H_2/Ar	1	1000 (MW)	250	[25]
500	$SiCl_4$/Ar	20	NM	400	[28]
330	$SiCl_4$/Ar	50	200 (RF)	NM	[31]

* MW designates a microwave power supply, whereas RF designates a radio frequency power supply.
\# NM designates a parameter that was not mentioned in the reference.

Ga, Al and In at the surfaces. Addition of a fluorine-containing gas (SiF_4) was added to their $SiCl_4$ plasma to facilitate removal of atomic nitrogen from the surface. As expected, this addition had no effect on the etch rate probably due to the competitive formation of GaF_x and volatile $GaCl_x$ at the surface.

Methane-based plasmas have been employed because of the speculation that methyl species and group III metal atoms, in this case Ga, will form a volatile metalorganic compound, such as trimethylgallium. Unfortunately, there is no mass spectrometer data to support this hypothesis. In general, etch rates of GaN are slow, as compared to chlorine-based plasmas, and a DC bias of about -175 V is required for initiation of the surface reaction.

More novel approaches to etching GaN have also been employed. Reactive fast atom beam etching was employed early on by Tanaka *et al.*[20] to etch GaN on sapphire in a Cl_2 plasma at substrate temperatures ranging between 80-150°C during etching. Etch rates of up to 1000-1200 Å/min produced relatively smooth surfaces and a well defined pattern of elongated rectangular bars. More recently, Adesida *et al.*[30] have employed chemically assisted ion beam etching to etch GaN with an Ar beam in a Cl_2 gas ambient. Results of their work should be available in the near future. Lastly, Pearton *et al.*[27] have employed a novel processing technique, called sidewall-etchback processing, to fabricate nanostructures of GaN as small as 300Å wide. This technique involves the following steps: photolithography of defined photoresist features, deposition of a thin (300-1000Å) layer of mask material (dielectric or metal) over the photoresist features, anisotropic etching of the mask leaving the vertical sidewalls intact, removal of the photoresist and anisotropic etching of the underlying GaN film. Dry etching in a $CH_4/H_2/Ar$ plasma (1 mtorr, -200 Vdc, 350 W microwave power) was employed to etch the GaN film slowly to preserve the integrity of the circular nanostructures. The etch-back technique is an important tool allowing one to produce sub-micron features without requiring advanced photolithography processing.

Etching of AlN. Aluminum nitride is a candidate material for optoelectronic devices because it possesses a high electrical resistivity, high thermal conductivity, low dielectric constant and has a direct transition bandgap of 6.3 eV[41]. AlN films have been grown by several techniques including CVD, MBE and ALE, and on a variety of substrate materials including sapphire, silicon, spinel, silicon carbide and quartz[42]. Etching fine features in the AlN films is an important step in the fabrication of such devices. AlN has been wet etched for various applications including synthesis of AlN powders from nitrided steels etched in $FeCl_3$[43] and development of piezolayer field effect transistors employing phosphoric acid[44]. In addition, mention of wet etchants, including NH_4F-based solutions[45, 46] NaOH solutions[47] hot H_3PO_4[48] and several other strong acids and bases[49], can be found in several Japanese patents regarding device fabrication. Our own research in the laboratory has shown that

significant weight loss of bulk AlN occurs when samples are immersed in high temperature solutions (T>100°C) of H_3PO_4, NaOH, KOH and LiOH solutions.

There have been a few reports of etching AlN in chlorine-based and methane-based plasmas by Pearton *et al.*[22, 23, 25]. High etch rates have been attained, as shown in Table II, especially for Cl_2/H_2 plasmas. As the case is for GaN, an increase in pressure produces an increase in the etch rate as a result of a high concentration of Cl at the nitride surface. In addition, the morphology of the etched surfaces becomes more smooth as the flow of H_2 is increased. This effect is thought to be the result of more efficient removal of the nitrogen etch product from the surface[25]. However, a threshold bias of about -100 V is required for removal of the native oxide and initiation of a surface reaction[23]. Examination of the AlN surfaces before and after etching, using AES, revealed no change in the stoichiometry, but a 2% atomic concentration of Cl was found on the surface. This would seem to indicate that slightly higher surface temperatures are necessary for complete removal of the $AlCl_x$ species.

Table II. Etch Rate Parameters for RIE of AlN

Maximum Etch Rate (Å/min)	Plasma Gases	Pressure (mtorr)	Microwave Power (watts)	DC Bias (-V)	Ref.
110	BCl_3/Ar	1	200	250	[23]
200	CCl_2F_2/Ar	1	200	300	[23]
25	$CH_4/H_2/Ar$	1	200	300	[25]
300	$CH_4/H_2/Ar$	1	1000	250	[25]
550	Cl_2/H_2	1	200	150	[25]
1100	Cl_2/H_2	1	1000	150	[25]

Etching of InN. Indium nitride also has a direct bandgap of 1.9 eV making it a promising candidate for visible light optoelectronic devices and high efficiency, low cost solar cells. Since the InN growth system is coming on line in our labs, it is desirable to be able to etch InN and fabricate patterned device structures. At the current time, wet etching has been accomplished by exposing (0001) InN samples to $NaOH/H_2O$ and KOH/H_2O solutions at temperatures between 20-60°C[50]. Etch rates of up to 600 Å/min and 300 Å/min at 60°C in KOH and NaOH, respectively, were achieved. Smooth surfaces free of etch pits were obtained, but no patterning was demonstrated.

Reactive ion etching has recently been employed to etch InN. Pearton *et al.*[22, 23, 25] have been conducting reactive ion etching on InN at low pressures (1-30 mtorr) in ECR discharges of chlorine- and methane based plasmas. Fairly high etch rates were attained at low pressure and high DC bias, as shown in Table III. With regard to chlorine-based plasmas, InN has a lower etch rate than GaN or AlN which can be attributed mainly to the low volatility of the $InCl_x$ species at normal cathode temperatures (around 25°C). Though significant heating of the samples can occur during etching by ion bombardment, the temperature of the samples surface is not high enough for the $InCl_x$ species to become volatile. The result is a rough, In-rich surface. AES results from Pearton's work[25] showed a nitrogen deficiency on the etched surface in addition to 6% atomic concentration of chlorine probably due to uncompleted reaction of Cl radicals with In atoms on the nitride surface. Interestingly enough, since the chlorine-based plasma produces fairly slow etch rates, relative to GaN and AlN, layers of InN could be used as etch stops for etching AlGaN/GaN heterostructures. Methane-based plasmas, on the other hand, require significant DC bias to obtain comparable etch rates (as compared to etch rates attained in Cl-based plasmas), i.e. a threshold bias of -175V was required before etch rate of 300 Å/min was attained[25]. High biases may induce significant damage to the surface, a characteristic that is undesirable for optimal device performance.

Table III. Etch Rate Parameters for RIE of InN

Maximum Etch Rate (Å/min)	Plasma Gases	Pressure (mtorr)	Power* (watts)	DC Bias (-V)	Ref.
175	BCl_3/Ar	1	200	300	[23]
300	Cl_2/H_2	1	200	300	[24]
190	CCl_2F_2/Ar	1	200	300	[24]
100	$CH_4/H_2/Ar$	1	200	300	[24]
350	$CH_4/H_2/Ar$	1	1000	250	[24]

Etching of Ternary Compounds. A low pressure (1 mtorr) ECR plasma discharge was employed by Pearton *et al.*[26] for reactive ion etching on $In_xGa_{1-x}N$ and $In_xAl_{1-x}N$ compounds. Etch rates were fairly high (≈ 200-350 Å/min) over the entire composition range even at high microwave power (1000 W) and DC bias (-250 V) when using a $CH_4/H_2/Ar$ plasma, but a slight increase in the etch rate (up to ≈ 400 Å/min) was observed with increasing In mole fraction. This behavior, Pearton believes, is a result of the In-methyl etch product

being more volatile than its Ga- and Al-methyl counterparts. Smooth surfaces and anisotropically etched features were observed over the whole range of composition. Higher etch rates were obtained for Cl_2/H_2 and Cl_2/SF_6 plasmas for low In mole fraction. As the In mole fraction decreased from 0% (all GaN and all AlN) to 100% (all InN), the corresponding etch rates dropped from 1000 Å/min and 700 Å/min, for $In_xAl_{1-x}N$ and $In_xGa_{1-x}N$ respectively, to 200 Å/min. Again, this result is expected since at high In mole fraction the $InCl_x$ species are more difficult to remove from the surface at normal cathode temperatures. More recently, Adesida *et al.*[30] have reported on reactive ion etching and chemically assisted ion beam etching of GaAlN. Details of their work have not yet been published.

C. Experimental Procedure

Experimental Apparatus. A schematic of the reactive ion etching system is shown in Fig. 1. The main components of the system include gas handling/storage, etcher, gas scrubber and mass spectrometer. Since toxic gases, such as BCl_3 and Cl_2, may be used to etch GaN and AlN, the system is designed for safe shutdown in the event of a power or water failure and/or inadvertent shutdown of the exhaust systems in the building.

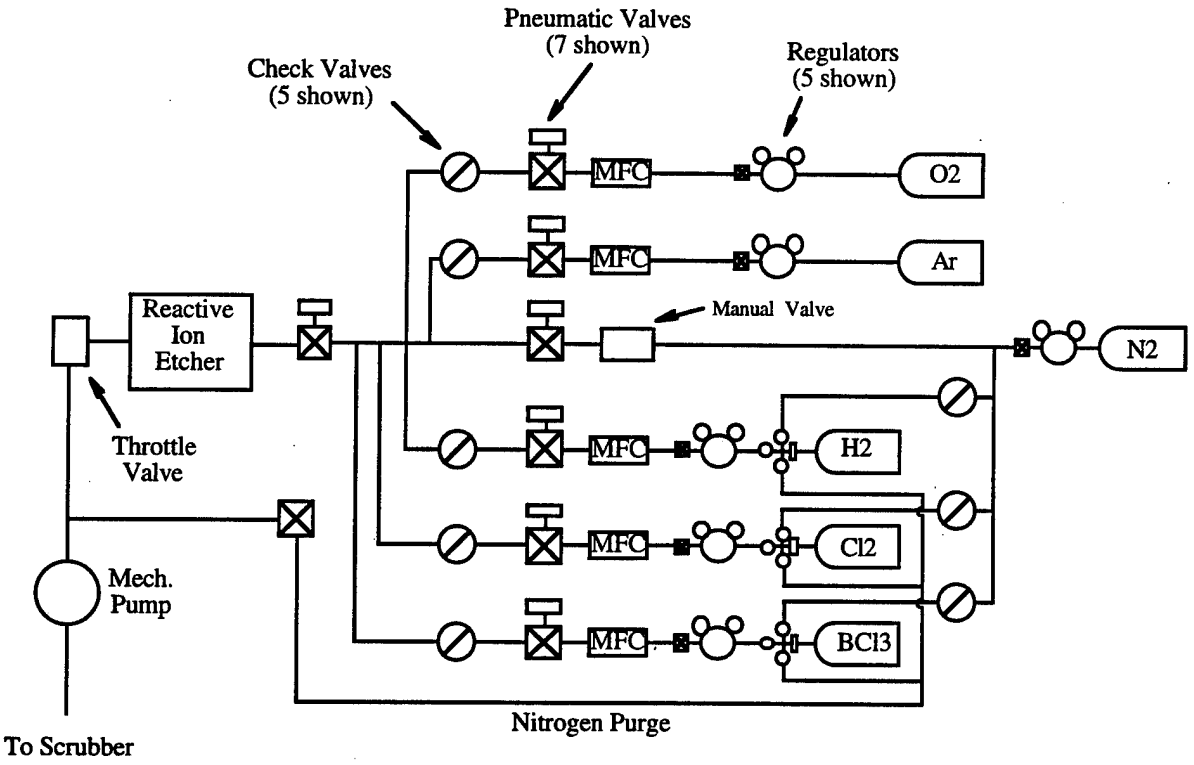

Figure 1. Schematic diagram of the reactive ion etching system.

The gas handling/storage sub-system consists of the gas storage cabinets, gas bottles, bottle regulators and necessary valves and tubing. Dry nitrogen is used to purge the gas lines before and after every run to remove moisture and chlorine from the lines, thus reducing the probability of corrosion of the gas lines. Mass flow controllers are employed for accurate control of the process gases. In the event of a power failure, interruption of the water supply or shutdown of the exhaust system, the solenoid actuated pneumatic valves will isolate the gas lines from the etch chamber.

The design of the etcher is based on that of the standard parallel-plate diode configuration, Fig. 2, in which the bottom electrode is powered by a RF power supply. The etcher, a Technics 85 series RIE, consists of an anodized aluminum chamber with an anodized aluminum water-cooled, driven lower electrode. A 350 Watt, 13.56 MHz RF generator with auto impedance matching network produces the power required to maintain a glow discharge in the chamber. The electrical potential applied across the parallel plate configuration results in ionization of the gas molecules, creating a plasma of neutrals, ions and electrons. Safety interlocks are supplied by Technics to disable the power when the system is vented or a panel is removed. The chamber pressure is measured by a capacitance manometer (absolute pressure) which is mounted to the underside of the chamber. The six channels of process gas (made from stainless steel tubing) are isolated from the injection manifold by means of air-operated electrically actuated isolation valves. In addition, an 19 CFM two-stage corrosive-series direct drive rotary vane pump provides the vacuum on the etch chamber.

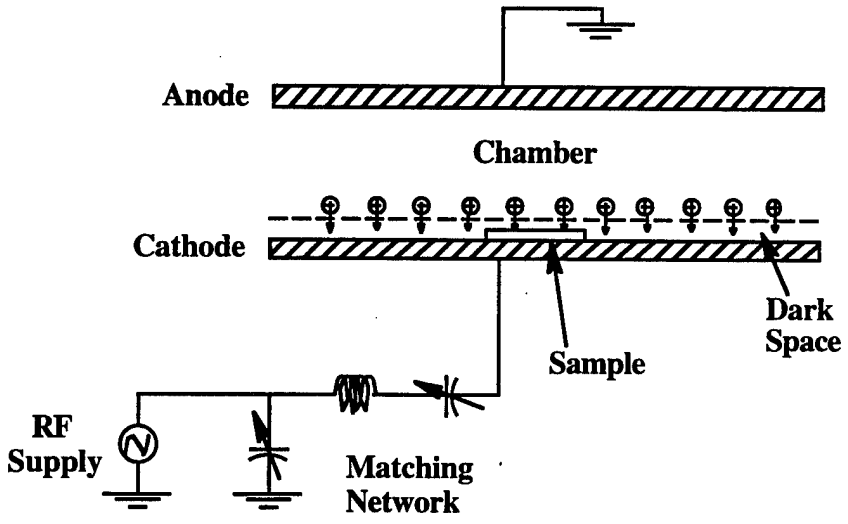

Figure 2. Schematic diagram of the parallel plate configuration.

Residual process gases and reaction by-products from the etcher will pass through a wet scrubber, which is equipped with a water recirculation line. These lines are monitored for water

flow and exhaust ventilation and are an integral part of the control system. Interruption of the water flow or inadequate ventilation will trip the pneumatic valves and close the gas lines. In addition, the pH level of the scrubber water is tested and monitored prior to each days etching runs.

Choice of Process Gases. There are a number of process gases that can be used to produce anisotropically etched features. For GaN, AlN and InN, fluorine plasmas are impractical because involitile fluorides are formed with Ga, Al and In at the surfaces, see Table IV, therefore limiting desorption of reaction species from the surface. Chlorine plasmas, on the other hand, have been used extensively for etching these compounds, see Section B above.

Table IV. Thermodynamic Data for Various Etchant Species

Species	ΔG_f^o (kJ/mole) at RT#	T_m(°C)*	T_b(°C)*
GaF_3 (g)	-1203	sublim. 800	-
$GaCl_3$ (g)	-565	78	201
AlF_3 (g)	-1530	sublim. 1291	-
$AlCl_3$ (g)	-738	sublim. 177	-
InF_3 (g)	-950	1170	> 1200
$InCl_3$ (g)	-475	sublim. 300	-

* From Reference [37].
\# From Reference [51].

Based on the success of Pearton *et al.* [22, 23] and others [20, 21, 28] Cl_2 and BCl_3 are currently being used as the main process gases in addition to Ar and N_2 as diluent and purge gases. The chlorine-based gases provide the following ionic and chemically reactive components via reaction of Cl_2 with electrons generated by the plasma:

$$Cl_2 + e^- \rightarrow Cl_2^+ + e^-$$

$$Cl_2 + e^- \rightarrow Cl^+ Cl + e^-$$

$$Cl_2 + e^- \rightarrow 2\,Cl + e^-$$

Experimentation with other gases, such as iodine- and/or bromine-containing gas mixtures and other chlorinated gases, is possible in order to obtain smooth, anisotropic features with reasonably high etch rates.

Etching Procedure. Prior to etching, low temperature processes are used to deposit thin layers of silicon dioxide (CVD) and nickel (thermal evaporation) to be used as a mask for patterning the nitride samples. Photolithography is then used to pattern the mask material. This involves spinning photoresist onto the masking layer, exposing unmasked areas of the resist to UV light and developing the resultant hardened resist. Exposed masking layer areas are etched away using wet chemical etchants and the resist is removed by acetone in an ultrasonic cleaner.

The RIE system is checked for proper water, air and exhaust supply. Samples are loaded into the etching chamber and process gas lines are pumped down to $\approx 5\times10^{-4}$ torr. A typical etch run includes the following steps:

1. Argon plasma to remove water vapor and hydrocarbon contamination from the sample and etch chamber,
2. Nitrogen purge to remove argon from etcher,
3. Cl_2/Ar or BCl_3/Ar plasma for processing,
4. Nitrogen purge to remove chlorinated process gases from the chamber,
5. Vent chamber to atmosphere with nitrogen.

After the samples are removed from the etcher, the mask is removed via wet chemical solutions and the step heights of the etched features are measured with a Detach stylus profilometer. In addition, SEM is used to observe the surface roughness and etched steps, and XPS and AES are used to observe the residual gas species on the sample surface.

D. Results

A reactive ion etching system has been installed and tested and is now operational. GaN has been etched in Cl_2/H_2, Cl_2/Ar and BCl_3/Ar plasmas with varying flow rates, pressures, power and DC bias. Typical etching parameters are: 1-10 sccm total gas flow, 35-75 mtorr, 125-200 W power and -(200-300)V bias. Etch rates of up to 200 Å/min and 150 Å/min have been achieved with Cl_2/Ar and BCl_3/Ar plasmas, respectively. Parametric studies are currently underway to optimize etching parameters employing Cl_2/Ar gas plasma. Etch rates of GaN thin films in Cl_2/H_2 plasmas vary with power, bias and pressure, as shown in Table V. Repeatability of the etch rate for a given set of etch parameters is also being studied.

E. Future Research

In the future, parametric studies will be continued to determine how the power, pressure, gas load and flow rates affect the etching rate of III-V nitrides in various chlorine-based

plasmas. Alternative Cl-containing gases such as methyl and nitrosyl chloride may be used in the future in order to establish etch rates of the nitrides and to study the underlying etch mechanisms. Surface analysis techniques such as AES and XPS will be employed to determine the contamination levels and surface condition of the nitrides before and after etching. In the future, scanning tunneling microscopy and atomic force microscopy may be employed to observe the surface morphology and to correlate etching parameters with surface damage. In addition, experimentation with different cathode materials (such as graphite and quartz) is possible if there is any micromasking from the cathode material. The ultimate goal of this research is to etch features necessary for optoelectronic and semiconductor devices fabrication.

Table V. Etch Parameters for Cl_2/H_2 Plasmas

Sample	sccm Cl_2	sccm H_2	pressure (mtorr)	power (W)	bias (-Vdc)	etch rate (Å/min)
1	1	3	50	100	236	-
2	5	3.3	75	150	205	60
3	2	2	50	100	214	11
4	3	1	50	100	231	13
5	1	1	25	250	370	70
6	5	3.3	75	200	218	30
7	2	1	25	200	285	40

F. References

1. *Plasma Processing of Materials: Scientific Opportunities and Technological Challenges*, National Research Council—Panel on Plasma Processing of Materials, Eds. (National Academy Press, Washington, D.C., 1991).
2. D. L. Smith, R. H. Bruce, J. Electrochem. Soc. **129**, 2045 (1978).
3. C. J. Mogab, A. C. Adams, D. L. Flamm, J. Appl. Phys. **49**, 3796 (1978).
4. L. M. Ephrath, J. Electrochem. Soc., (August 1979), 1419.
5. S. Matsuo, J. Vac. Sci. Technol. **17**, 587 (1980).
6. L. M. Ephrath, Solid State Technol., (July 1982), 87.
7. D. L. Smith, P. G. Saviano, J. Vac. Sci. Technol. **21**, 768 (1982).
8. Y. H. Lee, M. M. Chen, J. Appl. Phys. **54**, 5966 (1983).
9. M. Zhang, J. Z. Li, I. Adesida, E. D. Wolf, J. Vac. Sci. Technol. B **1**, 1037 (1983).
10. A. J. van Roosmalen, Vacuum **34**, 429 (1984).
11. J. W. Palmour, R. F. Davis, T. M. Wallett, K. B. Bhasin, J. Vac. Sci. Technol. A **4**, 590 (1986).
12. R. H. Bruce and G. P. Malafsky, J. Electrochem. Soc. **136**, 1369 (1983).
13. S. Park, L. C. Rathburn, T. N. Rhodin, J. Vac. Sci. Technol. A **3**, 791 (1985).

14. H. F. Winters, J. Vac. Sci. Technol. B **3**, 9 (1985).
15. D. A. Danner, D. W. Hess, J. Appl. Phys. **59**, 940 (1986).
16. N. N. Efremow, M. W. Geis, R. W. Mountain, G. A. Lincoln, J.N. Randall, N.P. Economou, J. Vac. Sci. Technol. B **4**, 337 (1986).
17. Y. Ochiai, K. Shihoyama, T. Shiokawa, K. Toyoda, A. Masuyama, K. Gama, J. Appl. Phys. **25**, L527 (1986).
18. R. J. A. A. Janssen, A. W. Kolfschoten, G. N. A. van Veen, Appl. Phys. Lett. **52**, 98 (1988).
19. G. Smolinski, R. P. Chang, T. M. Mayer, J. Vac. Sci. Technol. **18**, 12 (1981).
20. H. Tanaka, F. Shimokawa, T. Sasaki, T. Matsuoka, Optoelect. Dev. Technol. **6**, 150 (1991).
21. J. S. Foresi, M.S. Thesis, Boston University, Boston, MA, 1992.
22. S. J. Pearton, C. R. Abernathy, F. Ren, J.R. Lothian, P.W. Wisk, A. Katz, C. Constantine, Semicond. Sci. Technol. **8**, 310 (1993).
23. S. J. Pearton, C. R. Abernathy, F. Ren, J. R. Lothian, P. W. Wisk, A. Katz, J. Vac. Sci. Technol. A **11**, 1772 (1993).
24. C. R. Abernathy, F. Ren, S.J. Pearton, in *IEEE 6th International Conference on Indium Phosphide and Related Materials*, Eds. (IEEE, Piscataway, NJ, 1994), p. 387.
25. S. J. Pearton, C. R. Abernathy, F. Ren, Appl. Phys. Lett. **64**, 2294 (1994).
26. S. J. Pearton, C. R. Abernathy, F. Ren, Appl. Phys. Lett. **64**, 3643 (1994).
27. S. J. Pearton, F. Ren, C. R. Abernathy, J.R. Lothian, Semicond. Sci. Technol. **9**, 338 (1994).
28. I. Adesida, A. Mahajan, E. Andideh, Appl. Phys. Lett. **63**, 2777 (1993).
29. I. Adesida, A. T. Ping, C. Youtsey, T. Dow, M. Asif Khan, D. T. olsen, J. N. Kuznia, Appl. Phys. Lett. **65**, 889 (1994).
30. I. Adesida, A. T. Ping, in Eds. St. Louis, MO, 17-18 October 1994),
31. M. E. Lin, Z. F. Fan, Z. Ma, L. H. Allen, H. Morkoc, Appl. Phys. Lett. **64**, 887 (1994).
32. I. Akasaki, H. Amano, Physica B **185**, 428 (1992).
33. C. Eddy, Ph.D. Thesis, Boston University, Boston, MA, 1990.
34. T. Lei, T. D. Moustakis, J. Appl. Phys. **71**, 4933 (1992).
35. Z. J. Yu, B. S. Sywe, A. U. Ahmed, J. Electr. Mater. **21**, 782 (1992).
36. J. Sumakeris, Z. Sitar, K. S. Ailey-Trent, Thin Solid Films **225**, 244 (1993).
37. *CRC Handbook of Metal Etchants*, P. Walker, Eds. (CRC Press, Boca Raton, LA, 1991).
38. Y. Morimoto, J. Electrochem. Soc. **121**, 1383 (1974).
39. A. Shintani, S. Minagawa, J. Electrochem. Soc. **123**, 706 (1976).
40. V. V. Malinovskii, L. A. Marasina, N. V. Mitusova, I.G. Pichugin, Izv. Leningr. Elektrotekh. Inst. im. V. I. Ul'yanova **281**, 76 (1981).
41. E. S. Dettmer, B. M. Romenesko, H. K. Charles, B.G. Charkuff, D.J. Merrill, IEEE Trans. Comp. Hybrids Manuf. Technol. **12**, 543 (1989).
42. L. R. Rowland, Ph.D. Thesis, North Carolina State University, Raleigh, NC, 1992.
43. A. V. Omel'Chenko, M. A. Shelagarov, A. N. Frolov, M.E. Getmanova, G.S. Belousov, "Manufacture of Nitrides by Alloy Nitridation Followed by Selective Leaching," Small Enterprise Jilpa Ltd., Russia, PCT Int. Appl., 1992.
44. B. Matthes, E. Broszeit, O. Zucker, P. Gauer, Thin Solid Films **226**, 178 (1993).
45. M. Nagaoka, "Annealing Method for Compound Semiconductor Device Fabrication," Toshiba Corp., Japan, Jpn. Kokai Tokkyo Koho, 1987.
46. H. Kato, M. Sugata, T. Ikeda, "Manufacture of Silicon-Supported X-Ray Mask having Aluminum Nitride-Based Film," Canon K.K., Japan, Jpn. Kokai Tokkyo Koho, 1989.
47. A. Sasame, K. Shibata, H. Sakagami, "Aluminum Nitride Sintered Body with a Metalized Layer ans Its Manufacture," Sumitomo Electric Industries, Ltd., Japan, Jpn. Kokai Tokkyo Koho, 1986.
48. "Group IIIA Pnictide Semiconductor Device," Fujitsu Ltd., Japan, Jpn. Kokai Tokkyo Koho, 1982.

49. N. Yamaguchi, S. Ogawa, I. Yoshizawa, S. Kajita, K. Waki, "A Method for Manufacturing a Nitride-Type Ceramic Circuit Board," Matsushita Electric Works, Ltd., Japan, Jpn. Kokai Tokkyo Koho, 1986.
50. Q. X. Guo, O. Kato, A. Yoshida, J. Electrochem. Soc. **139**, 2008 (1992).
51. *HSC Chemistry* Program, Version 2.0, Outokumpu Research Oy, Inc., Pori, Finland, 1993.

VI. Distribution List

Mr. Max Yoder Office of Naval Research Electronics Division, Code: 312 Ballston Tower One 800 N. Quincy Street Arlington, VA 22217-5660	3
Administrative Contracting Officer Office Of Naval Research Resident Representative The Ohio State University Research Center 1960 Kenny Road Columbus, OH 43210-1063	1
Director, Naval Research Laboratory ATTN: Code 2627 Washington, DC 20375	1
Defense Technical Information Center Bldg. 5, Cameron Station Alexandria, VA 22314	2
Washington Headquarters Services ATTN: Dept. Acctg. Division Room 3B269, The Pentagon Washington, DC 20301-1135	2